“BABEŞ-BOLYAI” UNIVERSITY

FACULTY OF PHYSICS

Study of clusterisation process of rare earth ions in vitreous and ceramic matrices

PhD thesis abstract

Maria CLEJA (married Boşca)

Scientific supervisor:

Prof. Dr. Eugen CULEA

Cluj-Napoca, 2013

“BABEŞ-BOLYAI” UNIVERSITY

FACULTY OF PHYSICS

Study of clusterisation process of rare earth ions in vitreous and ceramic matrices

PhD thesis abstract

Maria CLEJA (married Boşca)

Scientific supervisor:

Prof. Dr. Eugen CULEA

Cluj-Napoca, 2013

THESIS OF CONTENT

Keywords:

Clusters, rare earth ions, spectroscopy, DTA, IR, RPE, magnetic susceptibility

INTRODUCTION

Glass is one of the oldest materials known to man. Thus, the oldest object made out of glass dates from 4000 B.C.

A long time, the glasses were used only for decorative purposes, but areas where glasses have found applicability expanded considerably with technological progress and theoretical concepts. In recent years, glasses have attracted considerable attention of researchers in that they exhibit interesting physical properties that lead to many technological applications such as lasers, fiber optics, semiconductor devices, photosensitive glass, radioactive waste storage, etc. Usability of the glasses appeared as knowledge about the structure and properties of glasses were enriched, especially in recent decades, as a result of modernization means of investigation and the development of theories necessary for a thorough study. To understand and control the properties they possess different vitreous and ceramic materials whose application areas are in constant development, of particular importance is the knowledge of existing local structure in such disordered systems, of how various technological factors that involved in their production process influences the type, structure and weight of the various structural units in which the interconnection network is performed chaotic glass.

GeO_2 is used for the production of new glasses with a wide range of applications mainly as a component in optical semiconductor devices, particularly integrated circuits and transistors. Due to the relatively high refractive index and dispersion properties of its optical material, glasses based GeO_2 as optical lenses and optical microscopes objectives. The crystalline GeO_2 shows several forms the most known being the quartz (where germanium atoms are tetra coordinated) and the rutile (where germanium atoms are hexa coordinated).

Glasses containing heavy metal oxides like PbO or Bi_2O_3 have attracted considerable attention of researchers in that they exhibit interesting physical properties that lead to many technological applications. These glasses have applications in optoelectronics in particular because of their high refractive index and low phonon energy. Bi_2O_3 and PbO are no traditional glass network formers, but in combination with other oxides can show this behavior.

Germanium and bismuth glasses are among the most studied oxide glasses with a vitreous matrix based on tetrahedrons linked together to form a continuous three-dimensional network. The basic structural units of the two vitreous networks (germanium and bismuth ones) are similar, despite the differences in bond lengths and angles and in the relative size of the bismuth and germanium atoms.

Glasses containing Ag_2O are studied due to their optical properties that provide multiple technological applications such as: diffractive elements, optical fiber, nanoplasmonic devices, sensors, bi- and nonlinear media, etc. Silver nanoparticles can be introduced in different environments: water solutions, polymers, crystalline environments, etc. Research on the formation of silver nanoclusters show numerous technical approaches. Between the investigations methods used some are based on ionizing radiation, that are interesting because of their ability to perform local or whole body irradiation. This type of analysis is used successfully in many branches of medicine.

On the other hand, the addition of rare earth oxides to the vitreous or ceramic materials gives them important magnetic, electrical and optical properties. Glasses and glass-ceramics doped with rare earth ions such as Er_2O_3, CeO_2, Eu_2O_3, Gd_2O_3, Nd_2O_3 and so on, have become an important class of materials, prompting the researchers' attention due to potential applications in various fields: telecommunications trough optical fiber, laser technology, ultrafast switching devices, etc. Considerable researches have been done, particularly focused on the infrared transmission of glass-ceramics and glasses, since they are essential components in the development of optical devices for lasers and signal amplifiers in telecommunications, optical fibers and for passive components associated to infrared spectroscopy by thermal imaging.

CHAPTER 1

GLASS STRUCTURES BASED ON Bi_2O_3 AND GeO_2

The local structure of the glasses can be understood from the crystallyne structure of the oxides contained in them. In the crystalline phase, the Bi_2O_3 presents four polymorphous phases, namely α, β, γ and δ, where the δ phase is stable only at high temperatures.

In the case of vitreous Bi_2O_3 obtained by melting quenching, the infrared absorption spectrum shows that the main structural units present in the glass network are the pyramidal units. In most of the binary or multicomponent glasses based on Bi_2O_3, spectroscopic techniques permit the identification of two types of structural units, the pyramidal BiO_3 units and the distorted octahedral BiO_6, present in varying proportions (Fig.1.1).

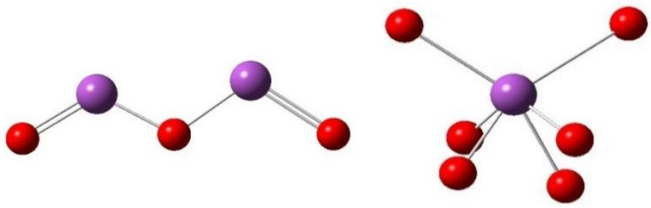

(a) **(b)**

Fig. 1.1. Structural units of vitreous Bi_2O_3: (a) BiO_3 pyramids and (b) octahedral BiO_6 units.

Germanium glasses are among the most studied oxide glasses. Their vitreous matrix is built up of tetrahedrons linked together to form a continuous three-dimensional network.

In the case of vitreous GeO_2 obtained by melting quenching, the IR absorption spectrum suggests that the glass is made up of pyramid units. In most binary or multicomponent glasses based on GeO_2, spectroscopic techniques identified two types of structural units, the GeO_4 pyramids and the distorted octahedral GeO_6 units, present in varying proportions (Fig.1.2).

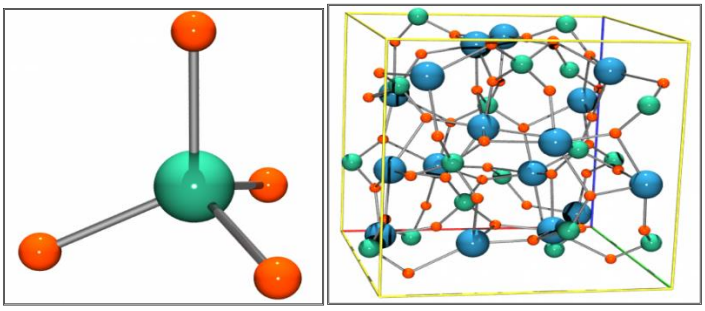

(a) **(b)**

Fig. 1.2. Structural units of vitreous GeO_2: (a) GeO_4 pyramids and (b) octahedral GeO_6 units.

The Ag_2O is an important additive used to confer interesting properties to the host glasses. Figure 1.3 presents the structure of Ag_2O.

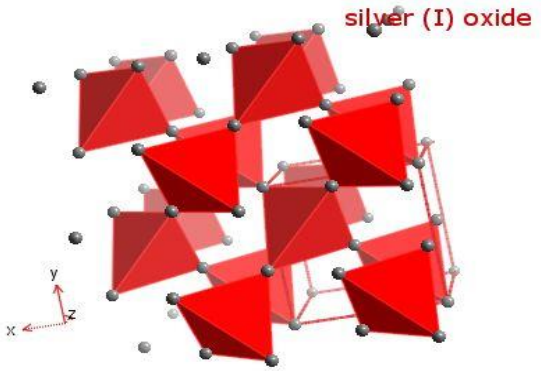

Fig.1.3. The structure of Ag_2O.

Under certain procedures (heat treatment, chemical methods, etc.), the silver atoms may give rise to nanoparticles in the glass matrix. The optical properties of glasses with silver nanoparticles presents many applications such as diffractive elements, optical filters, nanoplasmonic devices, sensors and multiple non-linear media.

We mention that the silver nanoparticles can be produced not only in glasses but in a variety of other environments such as aqueous solutions, polymers and crystalline media and all these materials are important due to their applications.

CHAPTER 2

INVESTIGATION METHODS UTILIZED TO STUDY VITREOUS SYSTEMS

Study of oxide glasses with rare earth ions aims to gather information on their structure and properties with the intention of contributing to the development of unified theories of vitreous solids and find new application fields. Next will be a summary of the study methods used in this paper, namely X-ray diffraction, infrared spectroscopy (FT-IR), density measurements, differential thermal analysis (DTA), magnetic susceptibility measurements and electron paramagnetic resonance spectroscopy (EPR) measurements.

CHAPTER 3

SAMPLES PREPARATION. INVESTIGATION TECHNICS

In order to study the behavior of rare earth ions (cerium, gadolinium, neodymium, erbium and europium) immobilized in various oxide vitreous matrices, new vitreous systems based on bismuth and germanium oxides were prepared. It was demonstrated that in these systems the rare-earth ions are positioned as a glass modifiers as well as glass formers. This arrangements allow to obtain homogeneous glasses of relatively high concentration of rare earth ions.

Thus, the following systems have been prepared and studied. Samples were obtained by themelt quenching method. To prepare the studied glasses p.a. purity oxides were used: GeO_2, Bi_2O_3, PbO, Ag_2O, CeO_2, Gd_2O_3, Nd_2O_3, Er_2O_3 and Eu_2O_3. These ingredients were mixed in the stoichiometric proportions, the obtained mixtures were placed in an electric furnace at a temperature of 1150°C for 15 minutes.

The crucibles used where made of sintered alumina. The cooling of the samples was carried out by pouring the melt on a stainless steel plate which was at room temperature.

Glass or ceramic structure of the samples was analyzed by X-ray diffraction measurements by using a Shimadzu 6000 equipment.

The IR transmission spectra were obtained by using samples prepared by the KBr pellet technique by using a JASCO FT-IR 6200 spectometer.

Magnetic susceptibility measurements were performed by using a Faraday type magnetic balance.

Density measurements of the samples was carried out by using of a pycnometer, which is a common method used to determine the density of solids.

Differential thermal analysis (DTA) investigation of the samples was performed using a termodiferential analysis (PerkinElmer TG/DTA 6300) equipment. The studied material and an inert reference are heated (or cooled) under the same conditions and recorded the temperature differences between sample and reference. This temperature difference is shown as a function of time or temperature, resulting in the DTA curve.

EPR measurements were performed at room temperature using a PS8400 Portable Adani spectrometer. The resonance phenomenon is obtained by scanning the static magnetic field in the region of interest.

CHAPTER 4

EXPERIMENTAL RESULTS FOR THE xRE·(100-x)[GeO_2·PbO],RE=CeO_2 OR Gd_2O_3 SYSTEM

4.1. The study of xCeO_2·(100-x)[GeO_2·PbO] system

4.1.1. X-ray diffraction

In Fig. 4.1 are presented the XRD diffractograms obtained for samples from the xCeO_2·(100-x) [GeO_2·PbO] system. The XRD patterns for the samples with $x \leq 1$ mol% shows the broad diffraction peaks specific to the amorphous structure. For samples with $x \geq 3$ mol%, the diffractograms show an overlapping of the broad peaks specific to the amorphous structure with some narrow peaks specific to crystalline phases.

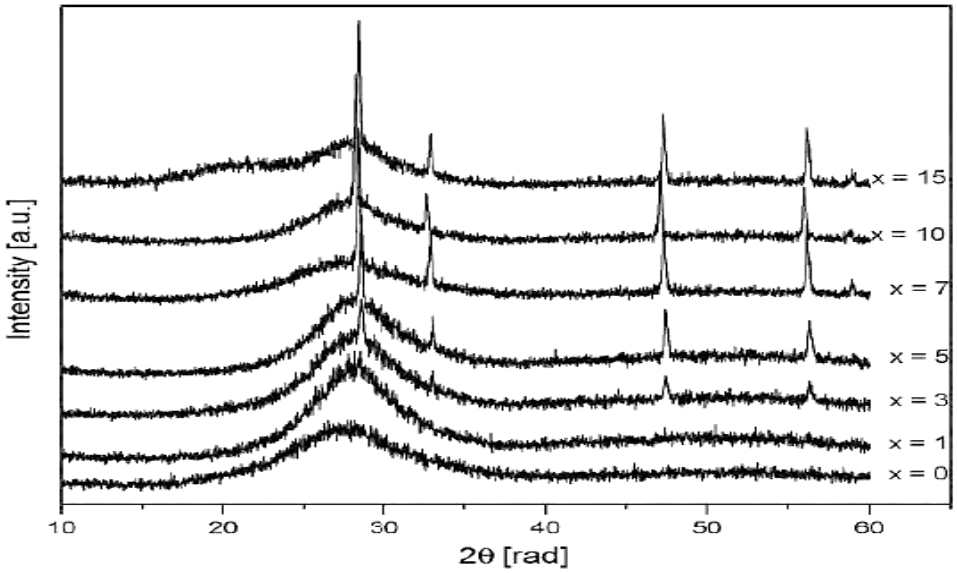

Fig. 4.1. XRD diffractograms for the $xCeO_2 \cdot (100-x)[GeO_2 \cdot PbO]$ system.

4.1.2. IR absorption spectroscopy

The obtained FT-IR spectra for the samples from the xCeO2·(100−x)[GeO_2·PbO] system with $0 \leq x \leq 15$ % mol are shown in Fig. 4.2. Since most of the IR bands present in these spectra are broad and asymmetric due to the amorphous (or partially amorphous) nature of the samples, it was necessary to use a de-convolution procedure of the experimental spectra.

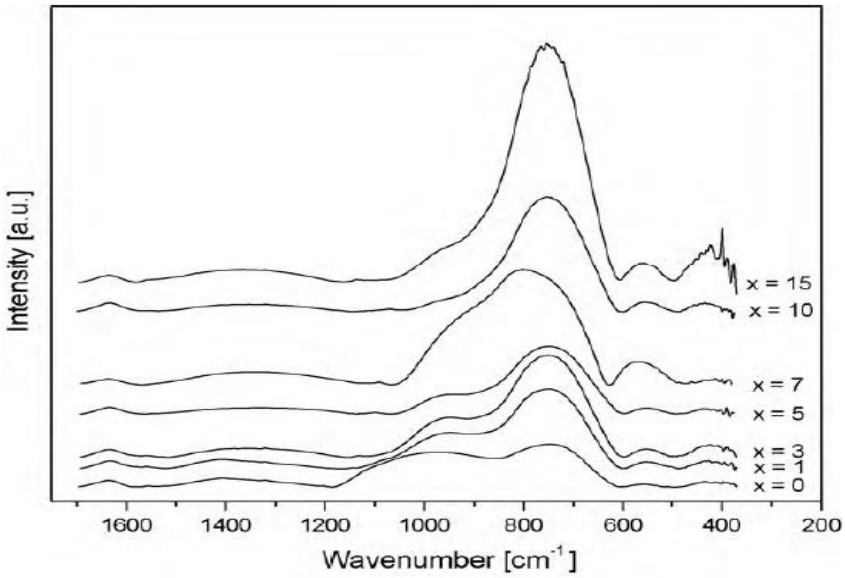

Fig. 4.2 IR spectra for xCeO2(100−x)[GeO2·PbO] system.

Increasing the concentration of CeO_2 of the samples affects the shape of the FT-IR spectra. This is due to structural modifications, sometimes including the apparition of

crystalline phase evidenced by XRD. Thus, with increasing the cerium content, the absorption bands at about 690 and 760 cm^{-1} become more intense and narrow. The bands at about 870 and 965 cm^{-1} decrease in intensity with the increase in of the cerium oxide content. These observations indicate two significant changes produced by increasing the concentration of CeO_2 in samples: (i) the gradual conversion of GeO_4 into more stable GeO_6 units and (ii) the decrease of vibrational modes number of symmetric stretching of the Pb-O bounds (linked to a vitreous matrix de-polymerization). These structural changes suggest an increase of the degree of the structural order in the samples with increasing the CeO_2 content, including due to the rise of the $Ce_{1.88}Pb_{2.12}O_{6.53}$ crystalline phase, highlighted by XRD.

4.1.3. Magnetic susceptibility

The experimental data obtained by magnetic susceptibility measurements show that the host vitreous matrix is diamagnetic. Thus, the magnetic behavior of the samples was assumed to be due to the presence of cerium ions. The cerium ions may be present in glasses in two valence state, 3+ and 4+. Ce^{3+} ions (electronic configuration of $4f^1$) are magnetic species with a magnetic moment of 2.56 μB while Ce^{4+} ions (without having unpaired electronic spin, with an electron configuration $4f^0$) are diamagnetic.

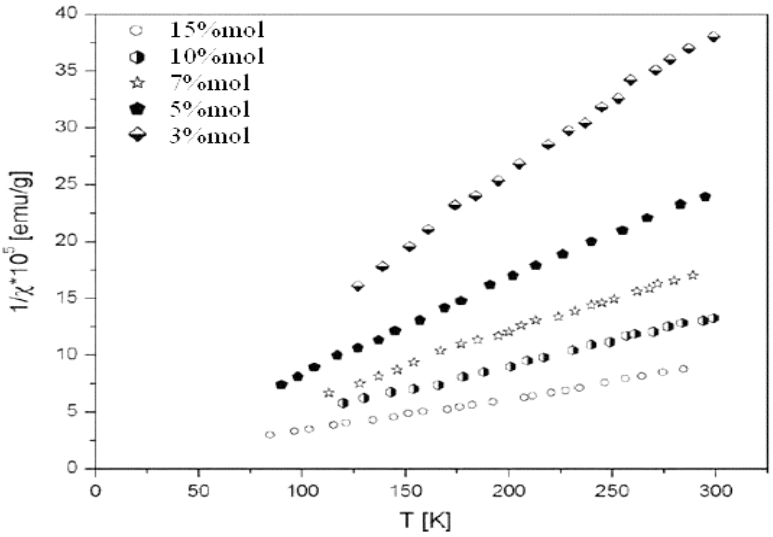

Fig. 4.3. Temperature dependence of the inverse magnetic susceptibility for the $xCeO_2 \cdot (100-x)[GeO_2 \cdot PbO]$ system.

Magnetic susceptibility measurements have allowed the determination of values the magnetic parameters important for describing the magnetic behavior of the studied samples: paramagnetic Curie temperatures, molar Curie constants and the effective magnetic moments of cerium 3+ ion (Table 4.1).

Table 4.1. Paramagnetic Curie temperatures, molar Curie constants and effective magnetic moments for $xCeO_2 \cdot (100-x)[GeO_2 \cdot PbO]$ system.

x [%mol]	$-\theta_p$ [K]	C_M [uem/mol]	μ_{eff} [μ_B/atom]
3	0	0,01275	1,84
5	3	0,02014	1,80
7	6	0,02814	1,79
10	10	0,03808	1,74
15	12	0,05744	1,75

Paramagnetic Curie temperature is an indicator of magnetic interactions between cerium ions. Negative values of θp, suggests the presence of antiferromagnetic interactions between the magnetic cerium ions. It is reasonable to assume that these are the super exchange interactions from the Ce^{3+}-O-Ce^{3+} bonds.

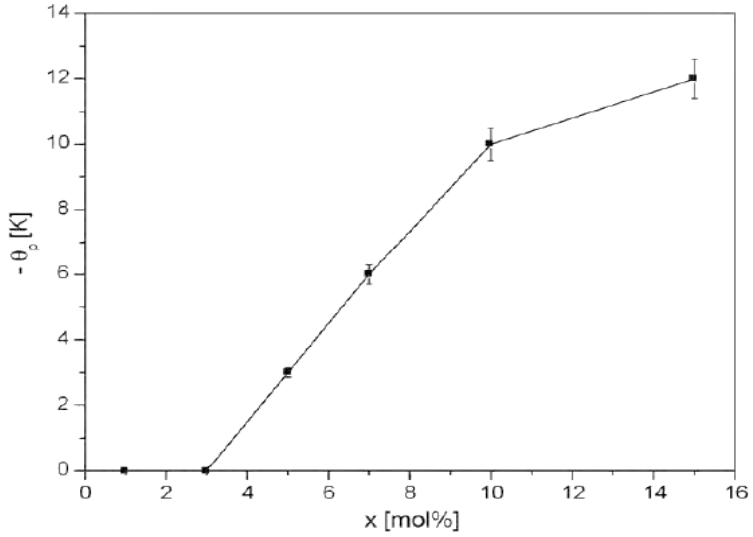

Fig. 4.4. Compositional dependence of the paramagnetic Curie temperature for the $xCeO_2 \cdot (100-x)[GeO_2 \cdot PbO]$ system.

4.2. Study of the $xGd_2O_3 \cdot (100-x)[GeO_2 \cdot PbO]$ system

4.2.1. X-ray diffraction

Fig. 4.5. presents the X ray diffractograms obtained for samples the from the $xGd_2O_3 \cdot (100-x)$ $[GeO_2 \cdot PbO]$ system with $0 \leq x \leq 10$ mol%. The diffraction patterns suggest that the samples with x <10 mol% are amorphous, while in the case of the sample with x=10 mol% a small amount of crystalline phase was detected, too.

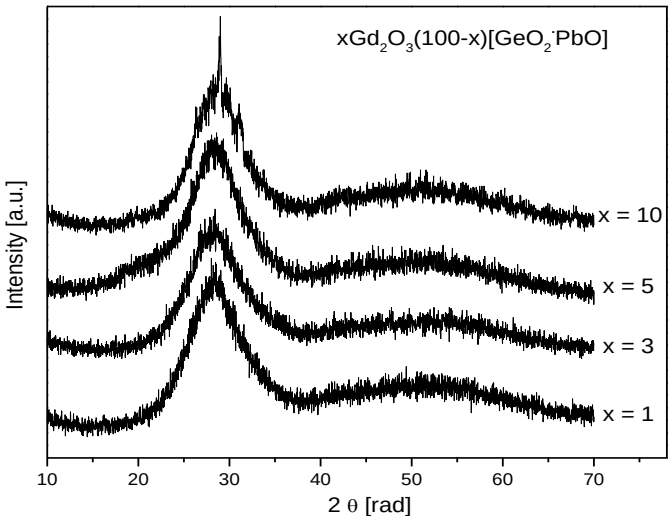

Fig. 4.5. X ray diffractograms for the $xGd_2O_3 \cdot (100-x)[GeO_2 \cdot PbO]$ system.

4.2.2. IR absorption spectroscopy

Fig. 4.6 shows the IR spectra of the samples from the $xGd_2O_3 \cdot (100-x)[GeO_2 \cdot PbO]$ system with $0 \leq x \leq 10$ mol%. The broad absorption bands shown in these spectra are in agreement with the amorphous nature of the samples, as suggested by XRD measurements, too.

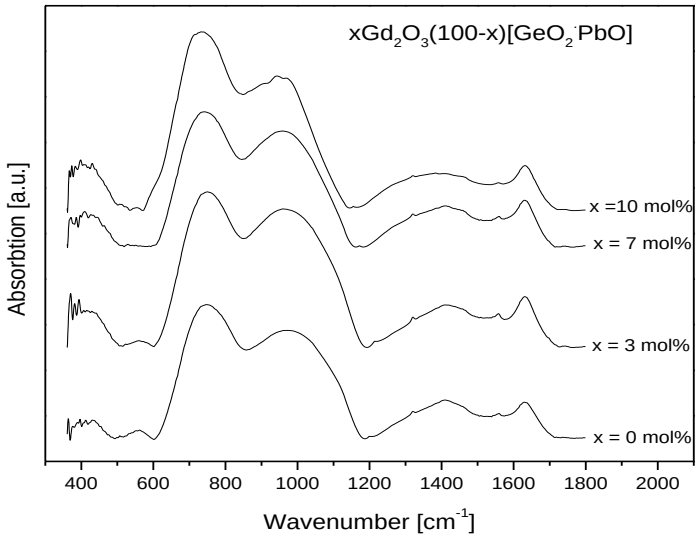

Fig. 4.6. IR Spectra for the $xGd_2O_3 \cdot (100\text{-}x)[GeO_2 \cdot PbO]$ system.

IR data analysis shows that the $GeO_2 \cdot PbO$ vitreous matrix is based on GeO_4, GeO_6 and PbO_4 structural units. Adding Gd_2O_3 seems to not produce significant changes on the IR spectrum of the $xGd_2O_3 \cdot (100\text{-}x)[GeO2 \cdot PbO]$ system. However, a trend was observed with increasing the Gd_2O_3 content for some IR bands.

The intensity of the absorption band located at about 550cm^{-1} decreases with increasing content of gadolinium oxide in the samples. This suggests that the addition of gadolinium ions in the germanium-lead glass matrix leads to a progressive depolarization of the vitreous network.

IR absorption bands located about 780 and 875 cm^{-1} are due to the asymmetric stretching vibrations of Ge-O-Ge bonds from the structural units GeO_4. The IR absorption band from about 700 cm^{-1} is due to the vibration of symmetrical stretching of the Ge-O-Ge bonds from the GeO_6 structural units.

Increasing the gadolinium content of the samples increases the intensity of the absorption band at ~700 cm^{-1} suggesting the increase of the number of GeO_6structural units. This is due to a conversion process of $GeO_4 \rightarrow GeO_6$.

The absorption band located at ~1395 cm^{-1} became broader with increasing the content of gadolinium oxide in the samples. This is explained by the increase of the deformation of the GeO_6 structural units with increasing gadolinium content in the samples.

4.2.3. Magnetic susceptibility

The temperature dependence of the inverse magnetic susceptibility for the $xGd_2O_3 \cdot (100\text{-}x)[GeO_2 \cdot PbO]$ system is shown in Fig. 4.7. The magnetic behavior of the studied samples is due to the presence of Gd^{3+} ions, which was reported in the case of other oxide glasses containing gadolinium ions, too.

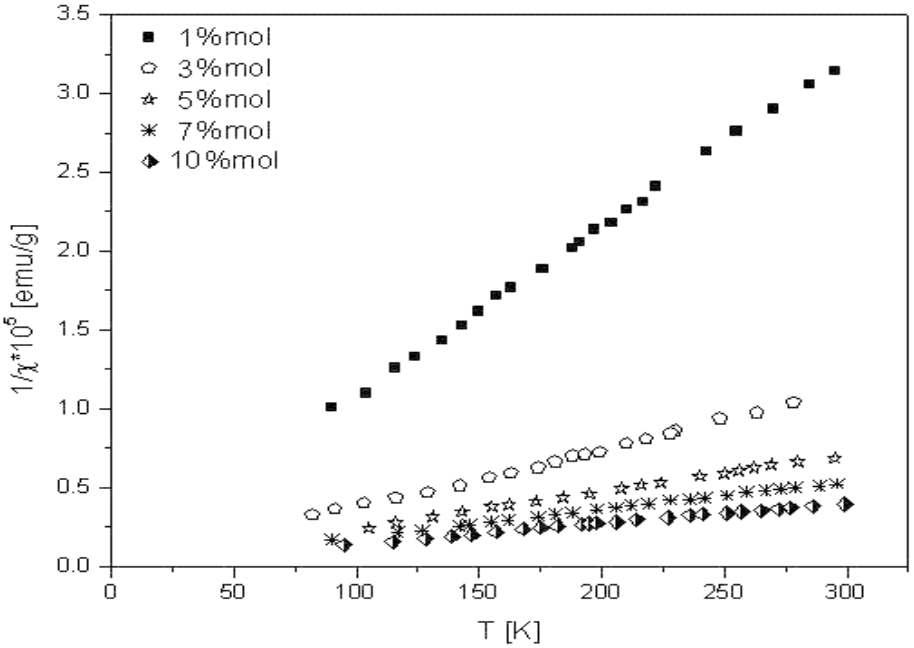

Fig.4.7. Temperature dependence of the inverse magnetic susceptibility for the $xGd_2O_3 \cdot (100-x)[GeO_2 \cdot PbO]$ system.

Magnetic susceptibility measurements have allowed the determination of important magnetic parameters such as the paramagnetic Curie temperature (θp), the molar Curie constant (CM) and the effective magnetic moment (μeff) which are presented in Table 4.4.

Sample containing 1 mol% Gd_2O_3 shows paramagnetic behavior since the thermal variation of the inverse magnetic susceptibility follows a Curie law. In this case, Gd ions are predominantly isolated or participate to dipole-dipole interactions. For $x \geq 3$ mol% Gd_2O_3, the temperature dependence of the inverse magnetic susceptibility follows the Curie-Weiss law with negative paramagnetic temperatures. Thus, for $x \geq 3\%$ mol glasses, gadolinium ions are coupled attending predominantly antiferromagnetic super exchange interactions (see Fig. 4.8 and Table 4.2).

Table 4.2. Paramagnetic Curie temperatures, molar Curie constants and effective magnetic moments for the $xGd_2O_3 \cdot (100-x)[GeO_2 \cdot PbO]$ system.

x [%mol]	$-\theta_p$ [K]	C_M [uem/mol]	μ_{eff} [μ_B/atom]
1	0	0,15533	7,88
3	1	0,46205	7,84
5	4	0,7453	7,72
7	6	1,01223	7,60
10	11	1,4115	7,51

Free Gd^{3+} ions show an effective magnetic moment of 7.94μB. Experimental Curie constants have allowed the determination of the values of magnetic moment per Gd^{3+} ion in the studied system. These values are close to each other, but slightly lower than that of the free Gd^{3+} ions and decrease with increasing the gadolinium content in the samples. This behavior is consistent with the antiferromagnetic nature of the interactions between gadolinium ions since antiferromagnetic interactions decrease the effective magnetic moment of gadolinium ions.

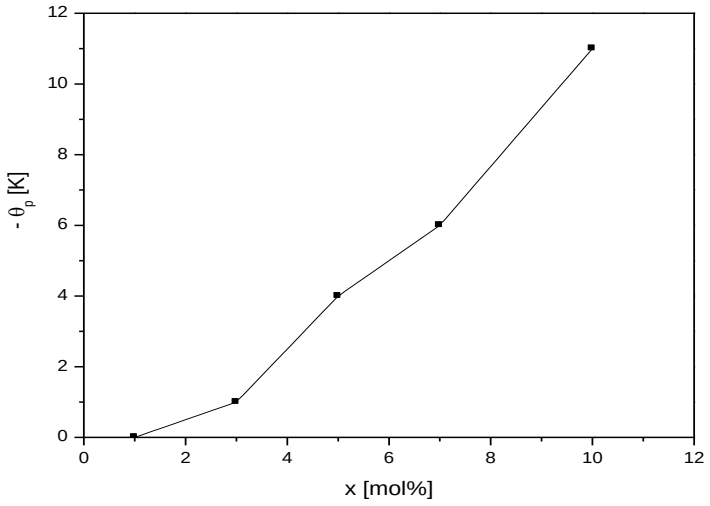

Fig. 4.8. Compositional dependence of the paramagnetic Curie temperatures for the $xGd_2O_3 \cdot (100-x)[GeO_2 \cdot PbO]$ system (the line is only a quide for the eye)..

In the studied samples, the magnetic interactions between the Gd^{3+} ions are super exchange interactions made via oxygen ions forming Gd^{3+}-O-Gd^{3+} pairs. With increasing

content of gadolinium ions in glass matrix, magnetic interactions between gadolinium ions lead to the creation of magnetic clusters in the glass matrix.

CHAPTER 5

EXPERIMENTAL RESULTS FOR THE $xEr_2O_3 \cdot (100-x)[72Bi_2O_3 \cdot 25PbO \cdot 3Ag_2O]$ SYSTEM

5.1. Study of the as cast $xEr_2O_3 \cdot (100-x)[72Bi_2O_3 \cdot 25PbO \cdot 3Ag_2O]$ system

5.1.1. X-ray diffraction

Fig. 5.1 shows the diffractograms obtained for samples from the as cast $xEr_2O_3 \cdot (100-x)[72Bi_2O_3 \cdot 25PbO \cdot 3Ag_2O]$ system.

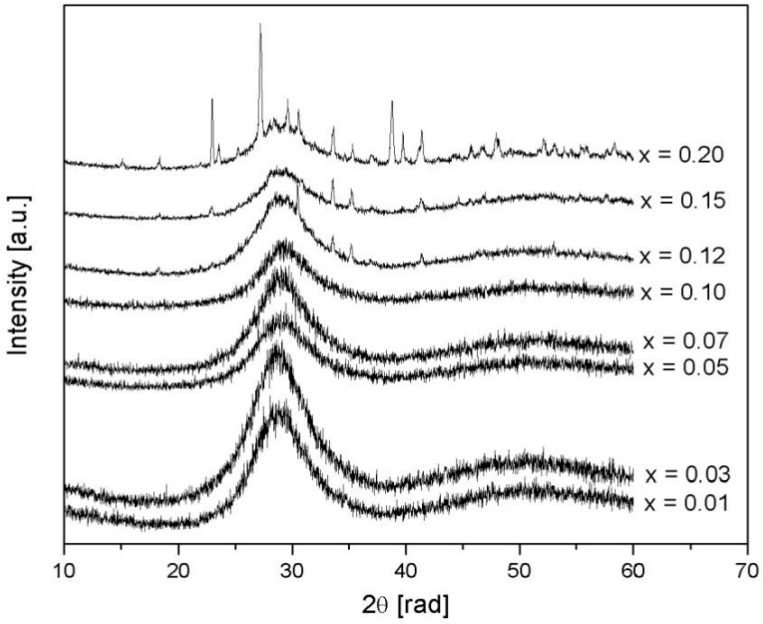

Fig. 5.1. X ray diffractograms for the as cast $xEr_2O_3 \cdot (100-x)[72Bi_2O_3 \cdot 25PbO \cdot 3Ag_2O]$ system.

One can see that for Er_2O_3 concentrations up to x = 10 mol% the obtained diffractograms are characteristic of amorphous structures, presenting a broad halo. For

samples with x ≥ 12 mol%, some additional diffraction peaks were observed suggesting that along the amorphous phase a crystalline phase occurs. These peaks increase in intensity with increasing Er_2O_3 content in the samples. The obtained XRD patterns were analyzed and it was found out that the mentioned crystalline phase is the δ-Bi_2O_3 one.

5.1.2. IR absorption spectroscopy

IR spectroscopy was used to obtain information on the structural units present in studied vitreous and ceramic systems.

The assignment of the IR absorption bands of the studied system was made taking into account the absorption bands fromt the IR spectra of the crystalline oxides of Bi_2O_3, PbO, Ag_2O and Er_2O_3 and the IR bands reported for other lead and bismuthate glasses.

The IR spectrum of the basic vitreous matrix, 72Bi2O3·3Ag_2O·25PbO, consists of three wide and intense absorption bands, located at ~480 cm^{-1}, ~722 cm^{-1} and ~890 cm^{-1}. However, in the spectrum of the host vitreous matrix, also occur several weaker bands located at ~510 cm^{-1}, ~560 cm^{-1}, ~669 cm^{-1}, ~850 cm^{-1}, ~960 cm^{-1} and ~1090 cm^{-1}.

The band at ~480 cm^{-1} may be due to the deformation vibration of Bi-O bond from units BiO_6 and/or BiO_3, as well to the Pb-O vibrations in PbO_4 pyramids.

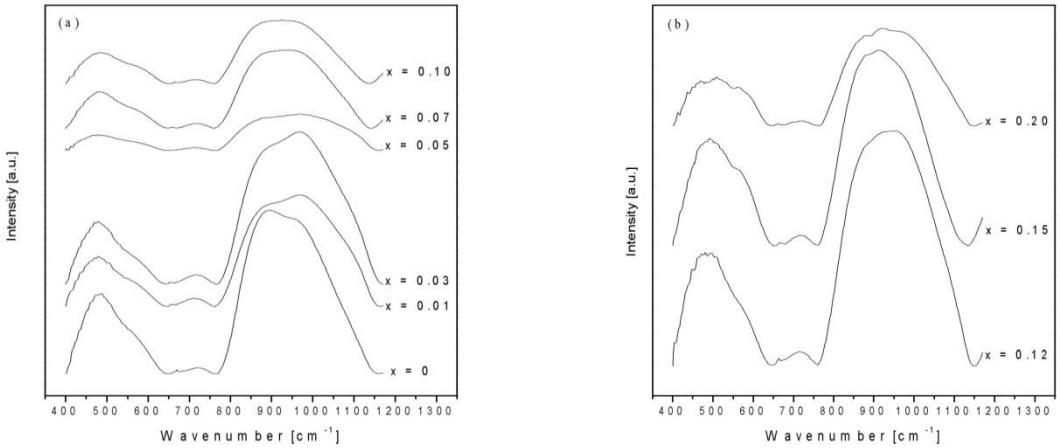

Fig. 5.2. IR spectra for the as cast xEr_2O_3·(100-x)[72Bi_2O_3·25PbO·3Ag_2O] system with 0 ≤ x ≤ 10 %mol (a) and 12 ≤ x ≤ 20 %mol (b)

The absorption band at ~510 cm^{-1} is may be assigned to the stretching vibrations of Bi-O bonds from the octahedral BiO_6 units as well as to the symmetric deformations of Pb-O

bonds. Absorption bands located at ~669 cm^{-1} and ~722 cm^{-1} are due to Pb-O vibrations from the PbOn structural units with n=3 and/or 4.

We mention that increasing the Er ions concentration of the samples, IR absorption bands become broader and lower in intensity. This is due to an increased structural disorder in the host glass matrix.

5.1.3. Magnetic susceptibility

For x>5 mol%, the temperature dependence of the inverse magnetic susceptibility is described by a Curie-Weiss law with a negative paramagnetic Curie temperature, θp. This magnetic behavior suggests that the neodymium ions from the studied samples are coupled antiferromagnetically. Thus, between these neodymium ions occurs super exchange interactions.

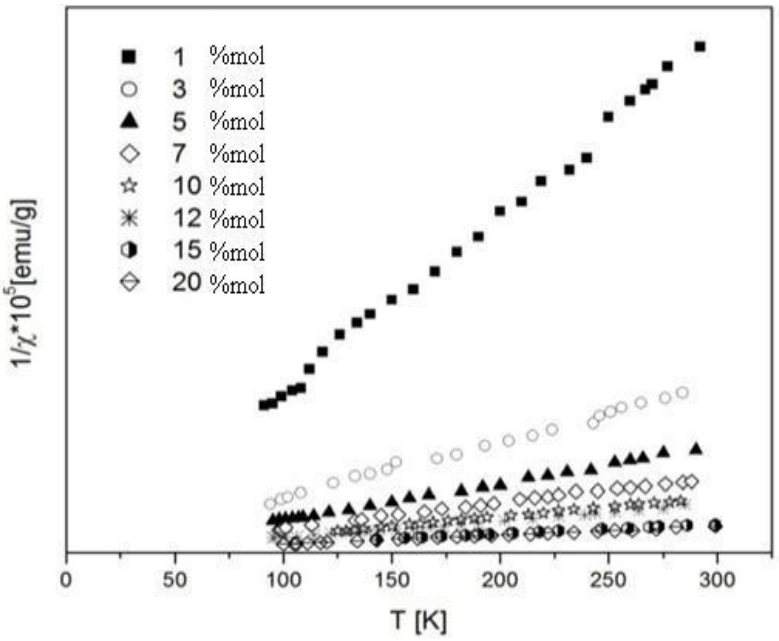

Fig. 5.3. Thermal dependence of the inverse magnetic susceptibilityfor the as cast $xEr_2O_3 \cdot (100-x)[72Bi_2O_3 \cdot 25PbO \cdot 3Ag_2O]$ system.

For samples with low concentrations of erbium ions it was observed that the temperature dependence of the inverse of the magnetic susceptibility respects the Curie type low. The change of the magnetic behavior of the glass system $xEr_2O_3 \cdot (100-x) \cdot [72Bi_2O_3 \cdot 25PbO \cdot 3Ag_2O]$ from the Curie type to the Curie-Weiss type one (with negative paramagnetic Curie temperatures), occurs around x=3mol% of Er_2O_3. This behavior suggests

that the erbium ions are present in the studied glasses as isolated species for x≤3mol% and as coupled species (by superexchange interactions of antiferromagnetic nature) for x>3mol%.

5.1.4. Differential thermal analysis

To determine the temperature recomanded for a heat treatment of the samples, the $xEr_2O_3 \cdot (100\text{-}x)$ [$72Bi_2O_3 \cdot 25PbO \cdot 3Ag_2O$] system with $0 \leq x \leq 20$ mol% was investigated by differential thermal analysis (DTA). DTA curves obtained at a heating rate of 20°C/min for the studied samples are shown in Fig. 5.4.

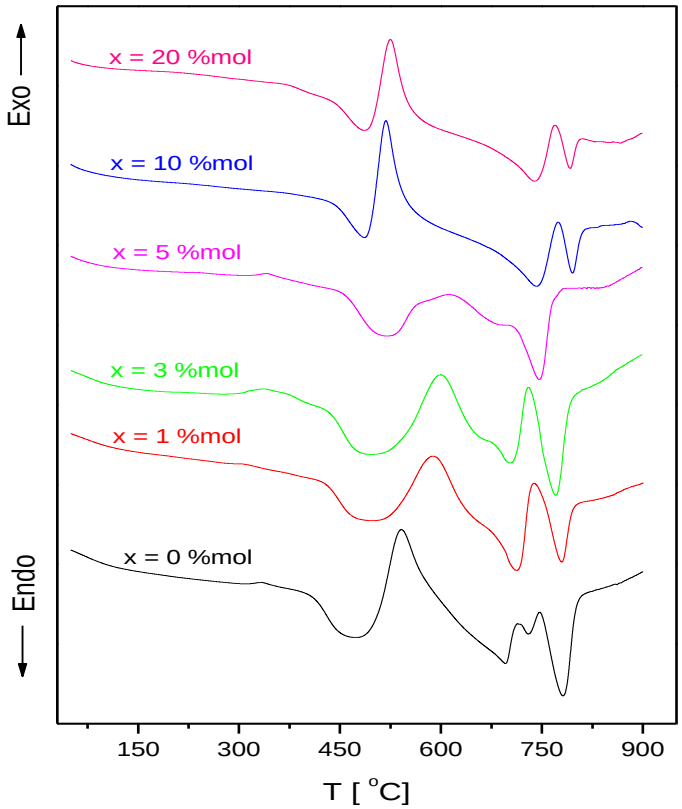

Fig. 5.4. DTA graphs obtained for the $xEr_2O_3 \cdot (100-x)[72Bi_2O_3 \cdot 25PbO \cdot 3Ag_2O]$ system.

The values obtained for the important thermal parameters of the investigated samples, namely the vitreous transition temperature (Tg), the crystallization temperature (T_{c1}, T_{c2}), and the melting temperatures (T_{m1} and T_{m2}) are presented in Table 5.2.

From the DTA graph for the basic glass matrix $72Bi_2O_3 \cdot 25PbO \cdot 3Ag_2O$ one can observe 5 thermal events: a vitreous transition at 433°C, a crystallization exothermic process at 541°C followed by endothermic signals at 696°C, 730°C and 782°C due to material melting in three stages. After analyzing the results obtained by the DTA measurements for the $xEr_2O_3 \cdot (100-x)[72Bi_2O_3 \cdot 25PbO \cdot 3Ag_2O]$ system with $0 \leq x \leq 20$ %mol, it was decided to submit these samples to a heat treatment performed at 650°C for 20 hours.

5.1.5. Density study

Density measurements for the $xEr_2O_3 \cdot (100-x)[72Bi_2O_3 \cdot 25PbO \cdot 3Ag_2O]$ system were performed using the picnometer method. With the experimental values obtained for the density, it can be determined Poisson's ratio which provide valuable information on the structural changes that occur with increasing the rare earth oxides content of the host glass matrix, $72Bi_2O_3 \cdot 25PbO \cdot 3Ag_2O$. Density, molar volume and Poisson's ratio of the studied samples is presented in Table 5.1 and figure 5.5.

Table 5.1.

Vitreous system		ρ [g/cm^3]	V_T [cm^3]	σ_{cal}
$[72Bi_2O_3 \cdot 25PbO \cdot 3Ag_2O]$		5,8126	0,313	0,0689
$xEr_2O_3 \cdot (100-x)[72Bi_2O_3 \cdot 25PbO \cdot 3Ag_2O]$	1	6,2450	0,345	0,0999
	3	6,2998	0,349	0,1074
	5	6,3128	0,353	0,1062
	7	6,4808	0,361	0,1190
	10	6,5250	0,365	0,1235
	15	6,5615	0,368	0,1278
	20	6,4805	0,365	0,1234

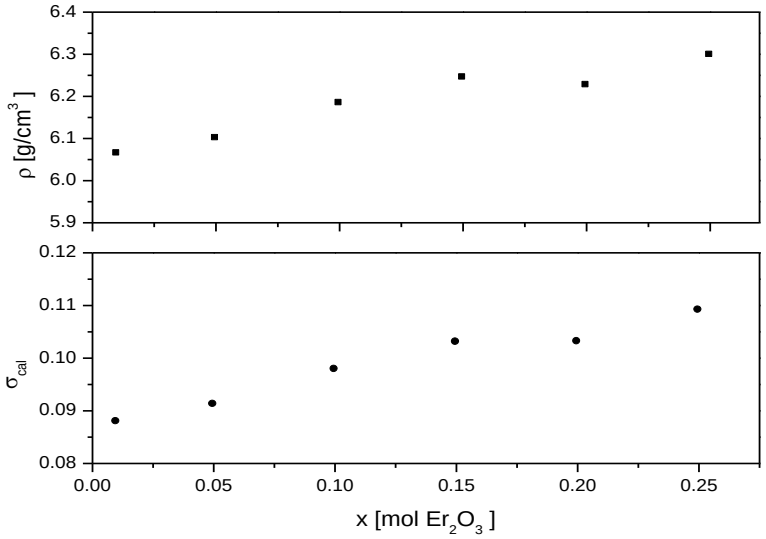

Fig. 5.5. Density dependency with Poisson index an concentration of Er_2O_3 for the as cast $xEr_2O_3 \cdot (100-x)[72Bi_2O_3 \cdot 25PbO \cdot 3Ag_2O]$ system.

By increasing the Er_2O_3 oxide content of the sample the packing density increases. The Poisson's ratio coefficient increase is due to the increase of ionic bonds share in the vitreous matrix where covalent bonds are predominant. The increase of the Poisson coefficient suggests the increase of the glass stiffness with increasing the rare earth oxide content of the samples.

Thus, as suggested by the IR spectroscopy, X-ray diffraction, magnetic susceptibility measurements and density data, we conclude that the addition of rare earth ions induce some structural changes in the host glass matrix.

5.2. Study of the heat treated $xEr_2O_3·(100-x)[72Bi_2O_3·25PbO·3Ag_2O]$ system

5.2.1. X-ray diffraction

After heat treatment the X ray diffractograms for all the samples show the occurrence and development of the Bi2O3 or PbO1, 44 crystalline phases as seen in Fig. 5.6.

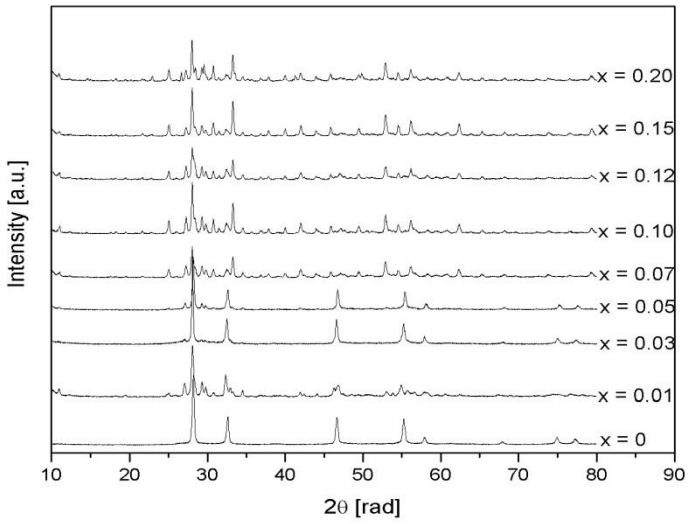

Fig. 5.6. Diffractograms for the heat treated $xEr_2O_3·(100-x)[72Bi_2O_3·25PbO·3Ag_2O]$ samples.

For the samples with x ≤ 3mol%, the X ray diffractograms show a single face-centered cubic phase with a lattice constant of 5.5Å. With increasing concentration of Er_2O_3 in samples, the characteristic peaks of this phase are gradually disappearing and new peaks

appear, most of which can be attributed to the face-centered cubic δ-Bi_2O_3 phase, with a lattice constants a=10.25Å.

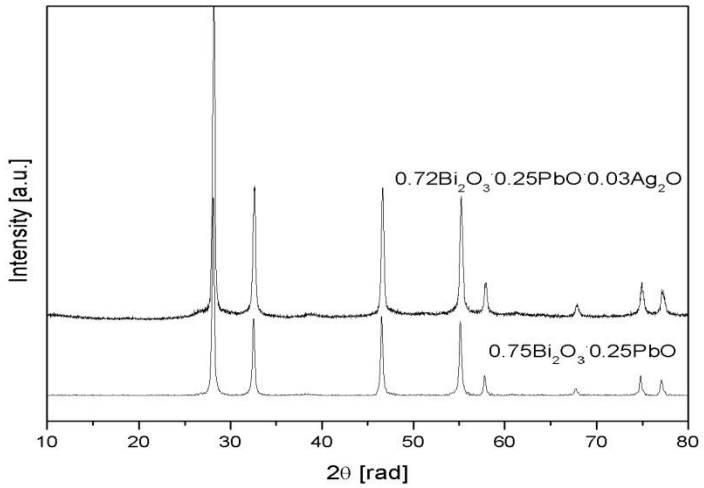

Fig. 5.7. X ray diffractograms for the heat treated $72Bi_2O_3 \cdot 25PbO \cdot 3Ag_2O$ and $75Bi_2O_3 \cdot 25PbO$ samples.

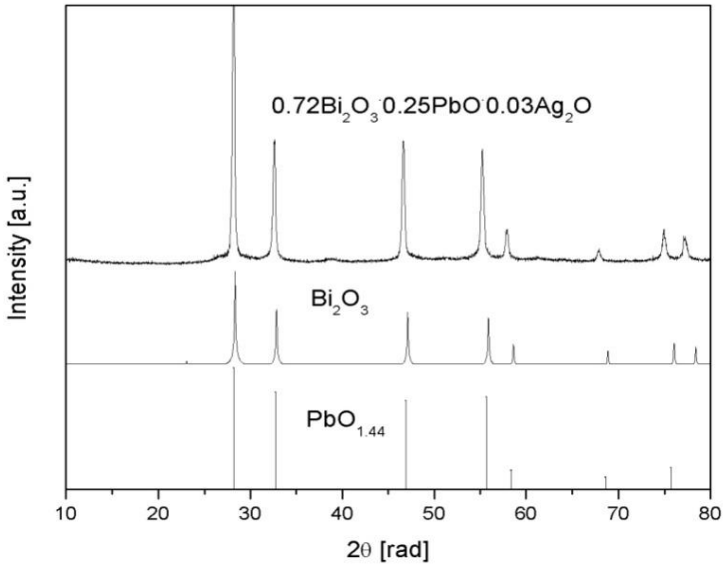

Fig. 5.8. X ray diffractograms for the heat treated $72Bi_2O_3 \cdot 25PbO \cdot 3Ag_2O$ sample and for the crystalline Bi_2O_3 and $PbO_{1,44}$.

5.2.2. IR spectroscopy

For the heat treated system, we can observe a narrowing of all IR spectral bands. This is due to the increase of the structural order associated with the crystallization which occurres during the heat treatment of samples (confirmed process of X-ray diffraction data). In the same time, the IR bands of the heat treated samples are easily shifted to higher wave numbers. Comparing the IR spectra of as cast and heat treated samples, we can note that there is a new peak for the treated samples, located at about 604 cm^{-1}. This peak is assigned to bending vibrations of Pb-O bonds.

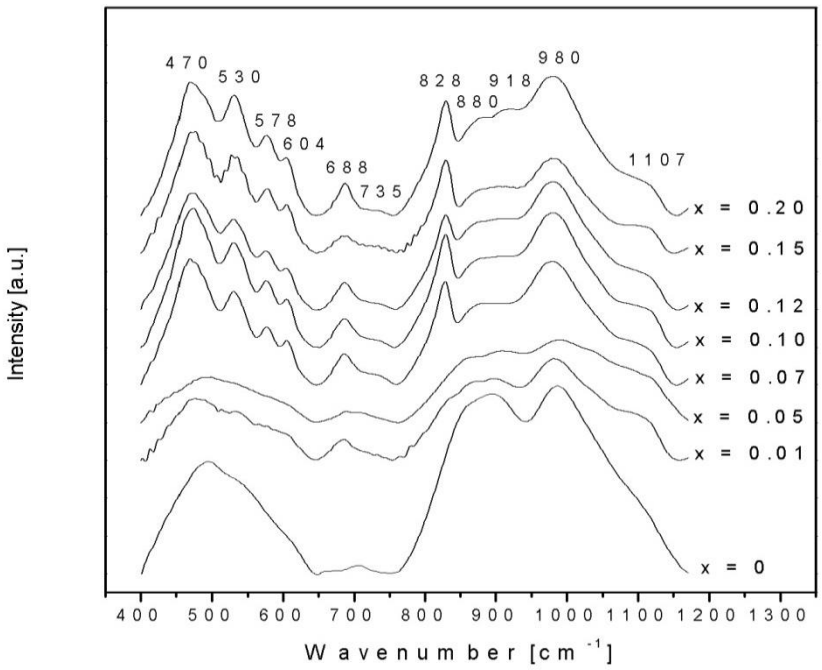

Fig. 5.9. IR spectra for heat treated $xEr_2O_3 \cdot (100\text{-}x)[72Bi_2O_3 \cdot 25PbO \cdot 3Ag_2O]$ system.

The most significant modification produced by the addition and increase of the of erbium ions content of the study samples consists in the increase in intensity of the FTIR bands from 688 cm^{-1} and 828 cm^{-1}, respectively the decrease in intensity for those located at 735 cm^{-1} and 880 cm^{-1}.

Thus, we can say that with increasing concentration of erbium oxide in the samples from system $xEr_2O_3 \cdot (100\text{-}x)[72Bi_2O_3 \cdot 25PbO \cdot 3Ag_2O]$, decreases the number of BiO_6 and PbO_3 structural units in favor of BiO_3 and PbO_4 units.

Structural changes observed from IR spectroscopy measurements for system $xEr_2O_3 \cdot (100\text{-}x)[72Bi_2O_3 \cdot 25PbO \cdot 3Ag_2O]$ suggest that erbium ion plays a network modifier role in the studied system.

5.2.3. Magnetic susceptibility

Magnetic susceptibility measurements are necessary to describe the magnetic behavior of the studied samples. The magnetic behavior of the $xEr_2O_3 \cdot (100\text{-}x)[72Bi_2O_3 \cdot 25PbO \cdot 3Ag_2O]$ system is due to the presence of erbium ions. In glasses, erbium participates in chemical combinations as trivalent ion having three 4f electron spins uncompensated. The free state Er^{3+} ion is characterized by a magnetic moment of 9.60 μB.

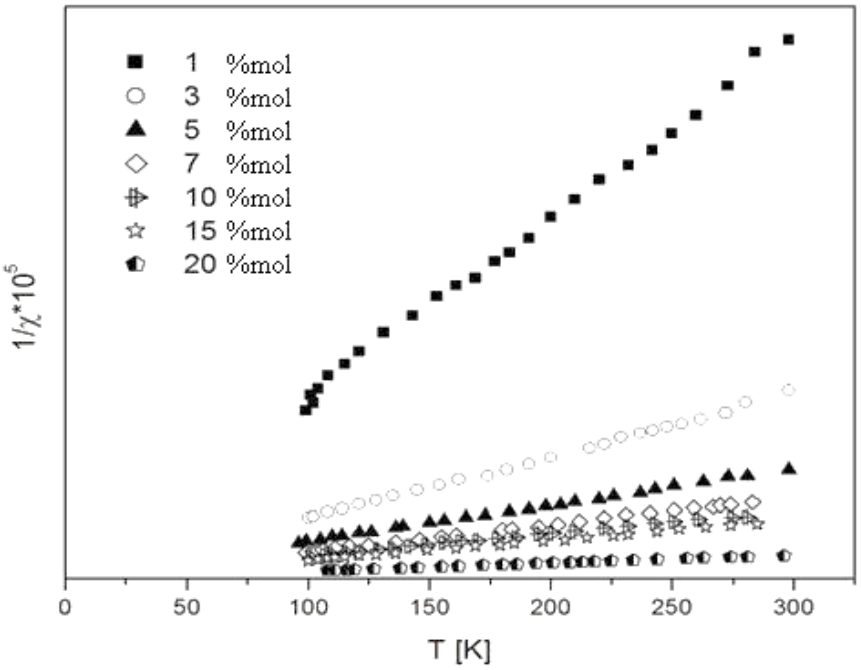

Fig. 5.10. Temperature dependence of the inverse magnetic susceptibility for the heat treated $xEr_2O_3 \cdot (100\text{-}x)[72Bi_2O_3 \cdot 25PbO \cdot 3Ag_2O]$ system.

Table 5.2. Paramagnetic Curie temperatures, molar Curie constants and effective magnetic moments for the heat treated $xEr_2O_3 \cdot (100-x)[72Bi_2O_3 \cdot 25PbO \cdot 3Ag_2O]$ system.

x [%mol]	$-\theta_p$ [K]	C_M [uem/mol]	μ_{ef} [μ_B/atom]
1	0	0,2215	9,39
5	1,6	1,1042	9,30
10	4	2,0849	9,11
15	6,3	3,1034	9,07
20	7,4	4,1215	9,04

The values of effective magnetic moments of erbium ion are lower than those of the erbium ion in the free state. Thus, we can say that in the studied samples the erbium ions appear both as isolated ion Er^{3+} or as ion pairs antiferromagnetic coupled through super-exchange interactions with an angle between the magnetic moments of erbium ions (antiferromagnetic coupling decreases the effective magnetic moment with increasing Er_2O_3 concentration.

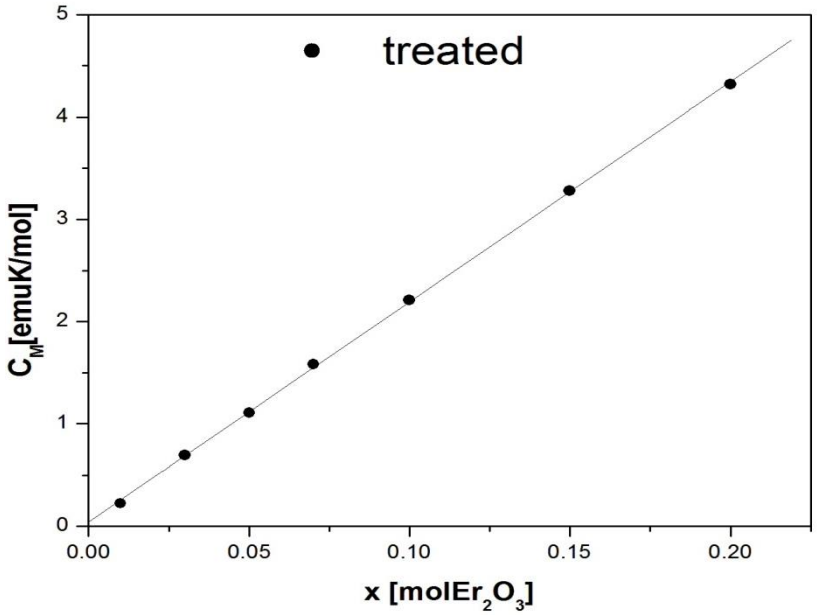

Fig.5.11. Compositional dependence of the paramagnetic Curie temperature for the heat treated $xEr_2O_3 \cdot (100-x)[72Bi_2O_3 \cdot 25PbO \cdot 3Ag_2O]$ system.

In conclusion, in the studied samples the interaction between erbium ions consists of short distance super-exchange type. This interaction is achieved through oxygen ions and leads to Er^{3+}-O-Er^{3+} coupled pairs. At higher erbium ion contents these interactions results in the formation of magnetic clusters.

CHAPTER 6

EXPERIMENTAL RESULTS FOR THE $xNd_2O_3 \cdot (100-x)[72Bi_2O_3 \cdot 25PbO \cdot 3Ag_2O]$ SYSTEM

6.1. Study of the as cast $xNd_2O_3 \cdot (100-x)[72Bi_2O_3 \cdot 25PbO \cdot 3Ag_2O]$ system

6.1.1. X-ray diffraction

The X ray diffractograms for $xNd_2O_3 \cdot (100-x)[72Bi_2O_3 \cdot 25PbO \cdot 3Ag_2O]$ system with $x \leq 7$ mol% show only a broad halo of diffuse scattering characteristic of the amorphous structure. For samples with greater concentrations, $x \geq 10$mol%, the diffractograms show the diffuse scattering characteristic of amorphous structure overlapped by some peaks characteristic of crystalline phases (Fig. 6.1). Most of these diffraction peaks are characteristic of the Bi_2O_3 crystalline phase.

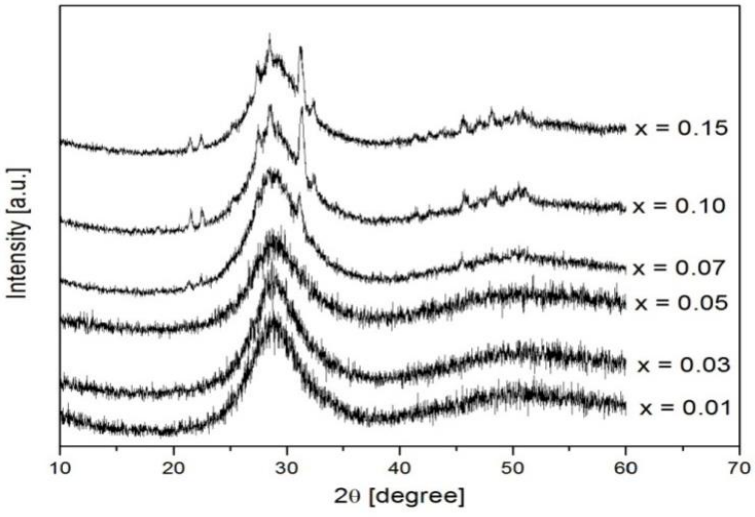

Fig. 6.1. Diffractograms for the as cast $xNd_2O_3 \cdot (1-x)[0,72Bi_2O_3 \cdot 0,25PbO \cdot 0,3Ag_2O]$ system.

6.1.2. IR spectroscopy

IR spectra were recorded for the bismuth-lead-silver glasses doped with neodymium ions, namely the $xNd_2O_3 \cdot (1-x)[0{,}72Bi_2O_3 \cdot 0{,}25PbO \cdot 0{,}3Ag_2O]$ system. These spectra are shown in Fig. 6.2.

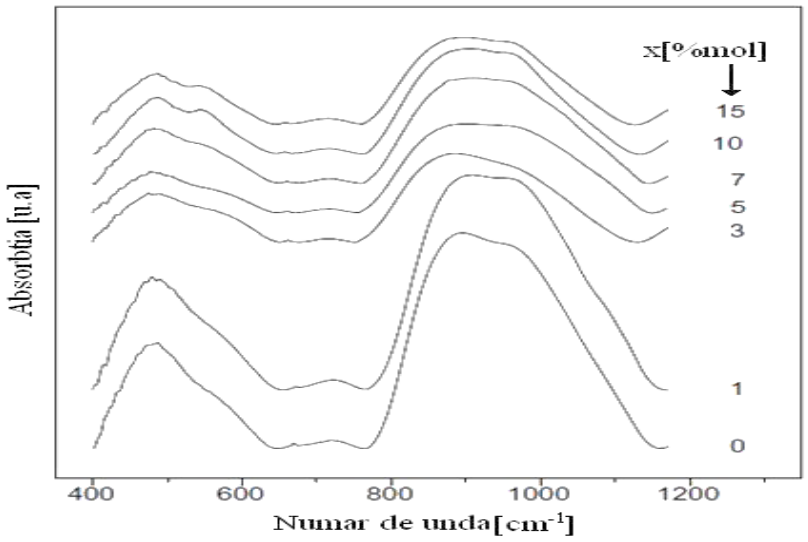

Fig. 6.2. IR spectra of the as cast $xNd_2O_3 \cdot (100-x)[72Bi_2O_3 \cdot 25PbO \cdot 3Ag_2O]$ system.

The obtained experimental IR spectra were subject of a deconvolution procedure in order to obtain a correct identification of the characteristic absorption bands. Figure 6.3 shows the result of the deconvolution procedure for the as cast sample with x = 15 %mol Nd_2O_3.

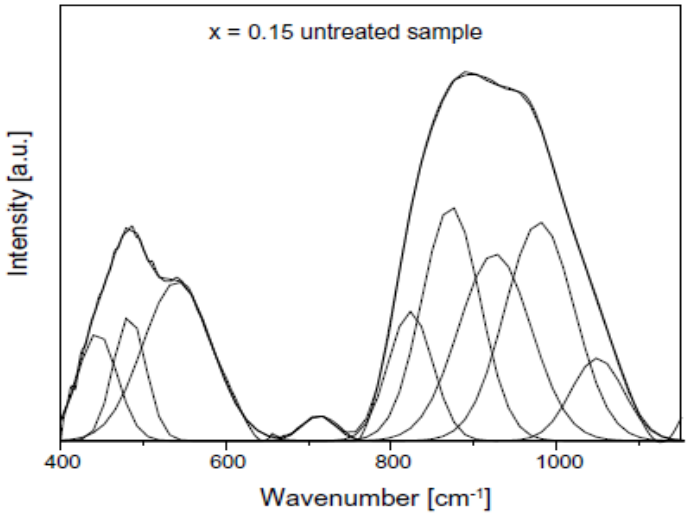

Fig. 6.3. Deconvolution of IR spectra for the as cast sample with x = 15 %mol Nd_2O_3.

The assignement of the characteristic IR bands was made by comparing the experimental spectra obtained with those of crystalline and vitreous related compounds that were previously reported. Thus, the IR spectrum of the basic vitreous matrix, $72Bi_2O_3 \cdot 25PbO \cdot 3Ag_2O$, consists of three wide and intense absorption bands, positioned at ~480 cm^{-1}, ~722 cm^{-1} and ~890 cm^{-1}. Some other weak absorption bands located at ~510 cm^{-1}, ~560 cm^{-1}, ~669 cm^{-1}, ~850 cm^{-1}, ~960 cm^{-1} and ~1090 cm^{-1} were observed, too.

In general, glasses based on Bi_2O_3 show five fundamental absorption bands positioned at about 890 cm^{-1}, 850cm^{-1}, 560cm^{-1}, 510 cm^{-1} and 480 cm^{-1}. Lead oxide also present five absorption bands located at about 1090 cm^{-1}, 960 cm^{-1}, 670 cm^{-1}, 722 cm^{-1}, 510 cm^{-1} and 480 cm^{-1}. Finally, the band at 560 cm^{-1} is associated with the presence of Ag-O bonds. The band at 480 cm^{-1} is characteristic of both Bi-O bending vibrations from structural units BiO_6 and BiO_3, and also Pb-O stretching vibration of PbO_4 units. The absorption band at 510 cm^{-1} is assigned to Bi-O stretching vibrations of the structural units BiO_6 and symmetric deformation vibrations of Pb-O bonds.

The absorption band at 560 cm^{-1} is due to the presence of structural units BiO_6 and vibrations bonds of Ag-O. Absorption bands located at 670 cm^{-1} and 722 cm^{-1} are due to vibrations of $Pb\text{-}O_n$, where n=3 and 4.

Addition of Nd_2O_3 to the basic host matrix produces changes of the IR spectra. These changes are associated with structural modifications and suggests a that the neodymium ions play a network modifier role in the host vitreous matrix.

6.1.3. Magnetic susceptibility

The temperature dependence of the inverse magnetic susceptibility of the as cast $xNd_2O_3 \cdot (100\text{-}x)\ [72Bi_2O_3 \cdot 25PbO \cdot 3Ag_2O]$ system is shown in Fig. 6.4.

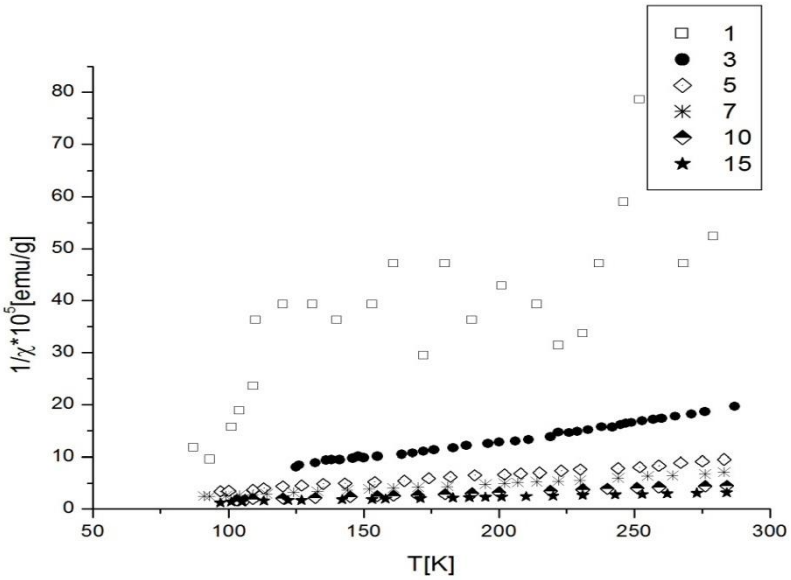

Fig. 6.4. Temperature dependence of the inverse magnetic susceptibility for the as cast $xNd_2O_3 \cdot (100\text{-}x)\,[72Bi_2O_3 \cdot 25PbO \cdot 3Ag_2O]$ system.

For samples with $x \leq 5$ mol% the temperature dependence of the inverse magnetic susceptibility is described by a Curie law. This suggests that the majority of the magnetic ions are present in the host matrix in the form of isolated species.

For samples with $x > 5$ mol% the temperature dependence of the inverse magnetic susceptibility is described by a Curie-Weiss law with negative paramagnetic Curie temperatures, θp. This magnetic behavior indicates that neodymium magnetic ions are present as species coupled through interactions of antiferromagnetic nature, namely super-exchange interactions.

6.1.4. Thermal differential analyses

The DTA curves for the samples of the as cast $xNd_2O_3 \cdot (100-x)[72Bi_2O_3 \cdot 25PbO \cdot 3Ag_2O]$ system with $0 \leq x \leq 10$ %mol, obtained for a heating rate of 20°C/min, are shown in Fig. 6.5.

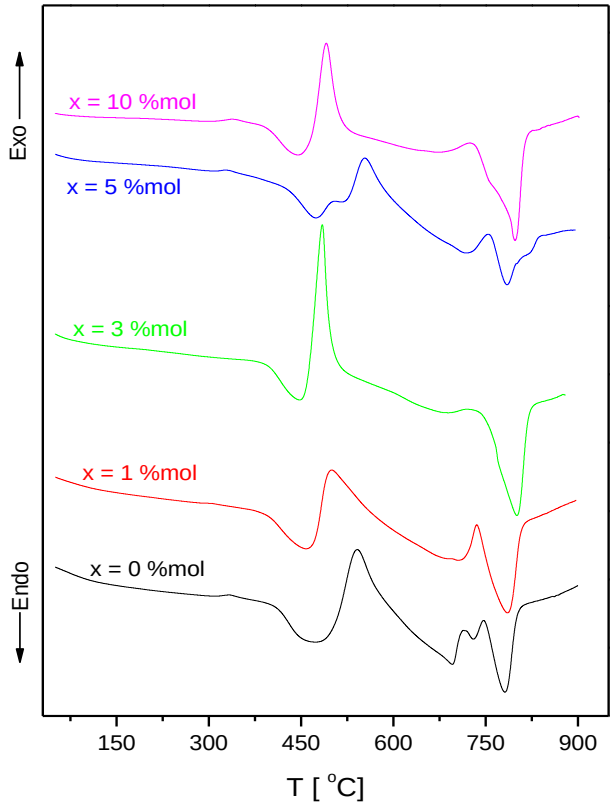

Fig. 6.5. DTA curves of the as cast $xNd_2O_3 \cdot (100-x)[72Bi_2O_3 \cdot 25PbO \cdot 3Ag_2O]$ system.

Experimental DTA curves allowed the determination of the important thermal parameters of the system $xNd_2O_3 \cdot (100-x)[72Bi_2O_3 \cdot 25PbO \cdot 3Ag_2O]$system: the vitreous transition temperature (T_g), the crystallization temperatures (T_{c1}, T_{c2}) and the melting temperatures (T_{m1}, T_{m2} and T_{m2}). These values are presented in Table 6.1.

Table 6.1. Vitreous transition temperature (T_g), crystallization temperatures (T_{c1}, T_{c2}) and melting temperatures (T_{m1}, T_{m2} and T_{m2}) for the as cast $xNd_2O_3 \cdot (100-x)[72Bi_2O_3 \cdot 25PbO \cdot 3Ag_2O]$ system.

x [%mol]	T_g [ºC]	T_{c1} [ºC]	T_{c2} [ºC]	T_{m1} [ºC]	T_{m2} [ºC]	T_{m3} [ºC]
0	433	541	-	696	730	782
1	423	500	-	685	707	786
3	417	484	-	676	690	801
5	452	502	554	720	785	820
10	414	491	-	640	674	796

For the studied samples it was observed that the addition of the neodymium ions in the host matrix $72Bi_2O_3 \cdot 3Ag_2O \cdot 25PbO$ decreases the temperature at which the glass transition takes place. I was observed also that the crystallization and melting also occurs in three steps. Baased on these results, we decided to submite the $xNd_2O_3 \cdot (100-x)[72Bi_2O_3 \cdot 25PbO \cdot 3Ag_2O]$ samples to a heat treatment at 600°C for 20 hours.

6.1.5. Density evaluation

The density of the $xNd_2O_3 \cdot (100-x)[72Bi_2O_3 \cdot 25PbO \cdot 3Ag_2O]$ samples was determined by the picnometer method. The experimental density values were used to obtain the Poisson coefficient values which provide valuable information on the structural changes that occur with the introduction of rare earth oxides in the host glass matrix, $72Bi_2O_3 \cdot 25PbO \cdot 3Ag_2O$. The addition of Nd_2O_3 generates the increase of the packing density. The Poisson's ratio increases from 0.0698 up to a maximum of 0.365 for x=25mol% Nd_2O_3. This increase of Poisson coefficient is due to a share increase of the ionic character of the bonds in the vitreous matrix where the covalent character is predominant. The compositional variation of the Poisson coefficient suggest a decrease of the glass rigidity with increasing the amount of neodymium oxide.

Table 6.4 presents the density, molar volume and Poisson ratio for the $xNd_2O_3 \cdot (100-x)[72Bi_2O_3 \cdot 25PbO \cdot 3Ag_2O]$ samples. Figure 6.6. presents the compositional dependence of density and Poisson coefficient.

Table 6.2. Density, molar volume and Poisson ratio for the $xNd_2O_3 \cdot (100-x)[72Bi_2O_3 \cdot 25PbO \cdot 3Ag_2O]$ samples.

Vitrous system		ρ $[g/cm^3]$	V_T $[cm^3]$	σ_{cal}
$[72Bi_2O_3 \cdot 25PbO \cdot 3Ag_2O]$		5,8126	0,313	0,0689
$xNd_2O_3 \cdot (100-x)$ $[72Bi_2O_3 \cdot 25PbO \cdot 3Ag_2O]$	1	6,0644	0,333	0,0873
	3	6,1005	0,338	0,0910
	5	6,1836	0,343	0,0972
	7	6,2445	0,347	0,1027
	10	6,2263	0,350	0,1025
	15	6,2980	0,351	0,1086

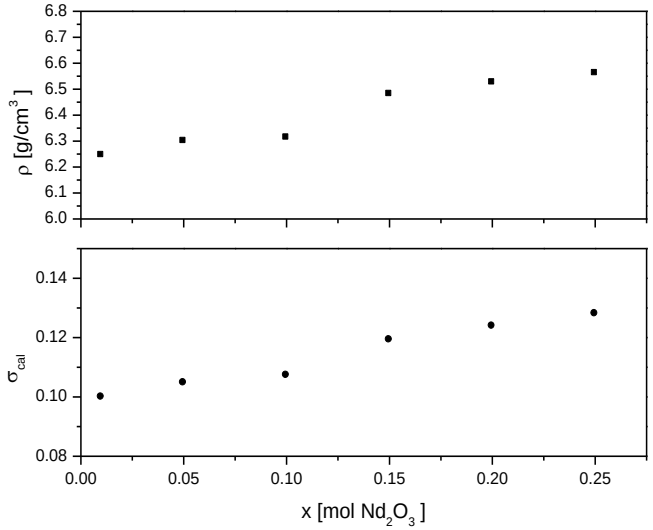

Fig. 6.6. Compositional dependence of density and Poisson coefficient.

Based on the experimental data obtained for the $xNd_2O_3 \cdot (100-x)[72Bi_2O_3 \cdot 25PbO \cdot 3Ag_2O]$ system, we conclude that the addition of neodymium ions induce some structural changes in the host vitreous matrix. This is supported by experimental data obtained by IR spectroscopy, X-ray diffraction and magnetic susceptibility and density measurements.

6.2. Study of the heat treated $Nd_2O_3 \cdot (100-x)[72Bi_2O_3 \cdot 25PbO \cdot 3Ag_2O]$ system

6.2.1. X-ray diffraction

The diffractograms for the heat treated $xNd_2O_3 \cdot (100-x)[72Bi_2O_3 \cdot 25PbO \cdot 3Ag_2O]$ system are shown in 6.7 and 6.8. These diffractograms show many peaks characteristic to crystalline phases that have been identified as belonging to the crystalline Bi_2O_3 and $PbO_{1,44}$. We note that in the heat treated samples the amorphous phase becomes minor.

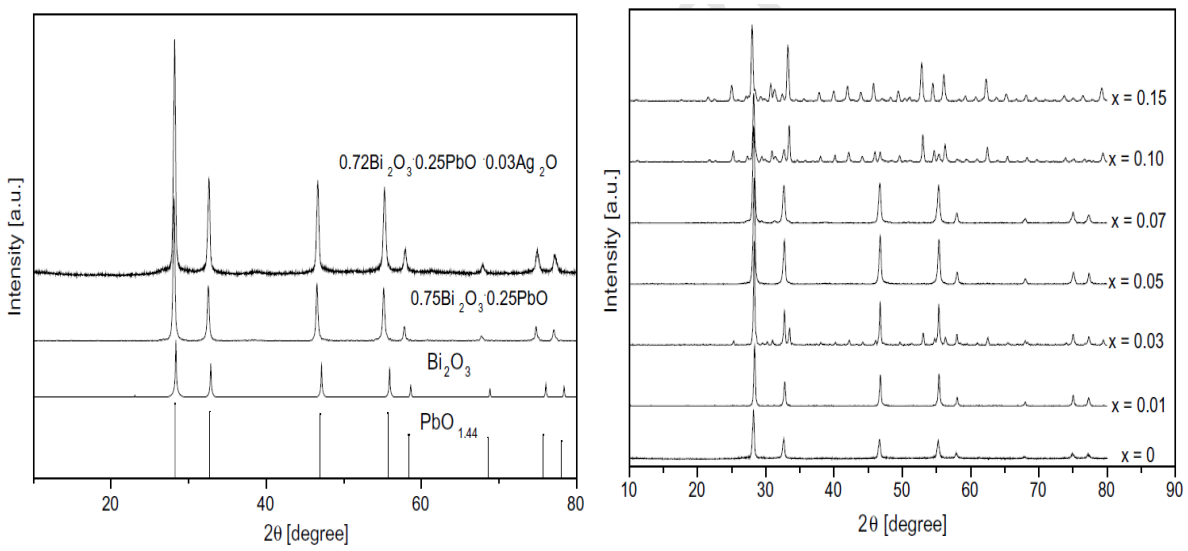

(a) **(b)**

Fig. 6.7. Diffractograms for (a) heat treated $72Bi_2O_3 \cdot 25PbO \cdot 3Ag_2O$ and (b) crystalline Bi_2O_3 and $PbO_{1,44}$.

6.2.2. IR absorbtion spectroscopy

The IR spectra of the heat treated samples present new absorption bands comparing to the spectra of the as cast samples. These new absorption bands are located at about 1030 cm^{-1}, 690 cm^{-1} and 605 cm^{-1}. Reshape of heat treated IR spectra is largely the result of the crystallization process that occurred in these samples after the thermal treatment.

Figure 6.8. presents the IR spectra of the heat treated $xNd_2O_3 \cdot (100-x)[72Bi_2O_3 \cdot 25PbO \cdot 3Ag_2O]$ system.

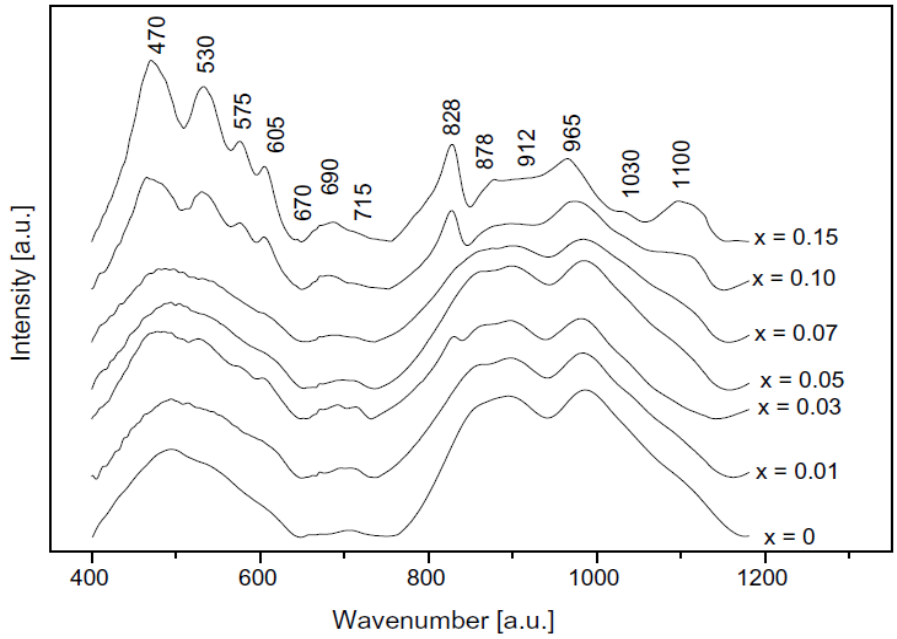

Fig. 6.8. IR spectra of the heat treated $xNd_2O_3 \cdot (100-x)[72Bi_2O_3 \cdot 25PbO \cdot 3Ag_2O]$ system.

The IR spectra for the heat treated $xNd_2O_3 \cdot (100-x)[72Bi_2O_3 \cdot 25PbO \cdot 3Ag_2O]$ system it can be observed a narrow and intense band located at about 605 cm^{-1}. This absorbtion band is attributed to asymmetric bending vibrations of the Pb=O bonds.

With the increase in the content of Nd_2O_3, there is an increase in the number of PbO_4 pyramidal units to the detriment of PbO_3 units. Thus, the band at ~690 cm^{-1}, increases in intensity, while the band at ~715 cm^{-1} decreases in intensity with increasing the Nd_2O_3 content of samples.

The IR absorption band at ~1030 cm^{-1} may be assigned to the PbO_4 and BiO_3 structural units. The absorption band at ~828 cm^{-1} decreases in intensity, compared to that located at 878 cm^{-1}.

FTIR spectroscopy studies show that the vitreous network matrix of the studied system contains the BiO_3, BiO_6, PbO_3 and PbO_4 structural units. Neodymium ions are introduced into the host matrix acting as a network modifier. Thus, Nd_2O_3 is responsible for the changes in the host matrix causing the conversion of BiO_6 into BiO_3 structural units and respectively of PbO_4 into PbO_3 structural units. After thermal treatment the samples show two crystalline phases, namely Bi_2O_3 and $PbO_{1,44}$, as was demonstrated by X ray diffraction investigations.

6.2.3. Magnetic susceptibility

Temperature dependence of the inverse magnetic susceptibility of the heat treated $xNd_2O_3 \cdot (100\text{-}x)[72Bi_2O_3 \cdot 25PbO \cdot 3Ag_2O]$ system is shown in Fig. 6.9.

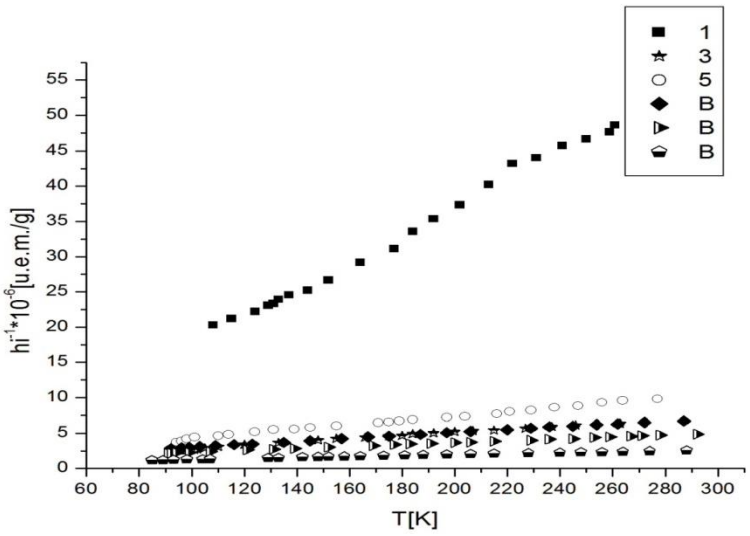

Fig.6.9. Temperature dependence of the inverse magnetic susceptibility for the heat treated $xNd_2O_3 \cdot (100\text{-}x)[72Bi_2O_3 \cdot 25PbO \cdot 3Ag_2O]$ system.

In Table 6.2 are shown the values of the key parameters that describe the magnetic behavior of the samples that were obtained from the experimental magnetic susceptibility data, namely the molar Curie constant, the magnetic moment per atom of Nd and the paramagnetic Curie temperature.

Table 6.2. Paramagnetic Curie temperatures, molar Curie constants and effective magnetic moments for the heat treated $xNd_2O_3 \cdot (100\text{-}x)[72Bi_2O_3 \cdot 25PbO \cdot 3Ag_2O]$ system.

x [%mol]	$-\theta_p$ [K]	C_M [uem/mol]	μ_{eff} [μ_B/atom]
5	2	0,1464	3,39
10	14	0,2764	3,28
15	19	0,3791	3,15
20	22	0,4977	3,12
25	23	0,6105	3,09

In general, in the vitreous oxidic system, neodymium ions occurs in a single valence state, Nd^{3+}, that is very stable. The Nd^{3+} ions presence in the studied samples causes the

apparition of their magnetic properties. We note that the free Nd^{+3} ion corresponds to an effective magnetic moment of 3.62μB/atom. Paramagnetic Curie temperature values are suggestive for the exchange interaction between magnetic ions. Figure 6.10 shows compositional dependence of the paramagnetic Curie temperature for the heat treated $xNd_2O_3 \cdot (100\text{-}x)[72Bi_2O_3 \cdot 25PbO \cdot 3Ag_2O]$ system. The estimated error in determining the paramagnetic Curie temperature is ± 2K. It is noted that the paramagnetic Curie temperature increases (in absolute value) with increasing concentration of neodymium ions over the entire range of investigated concentrations.

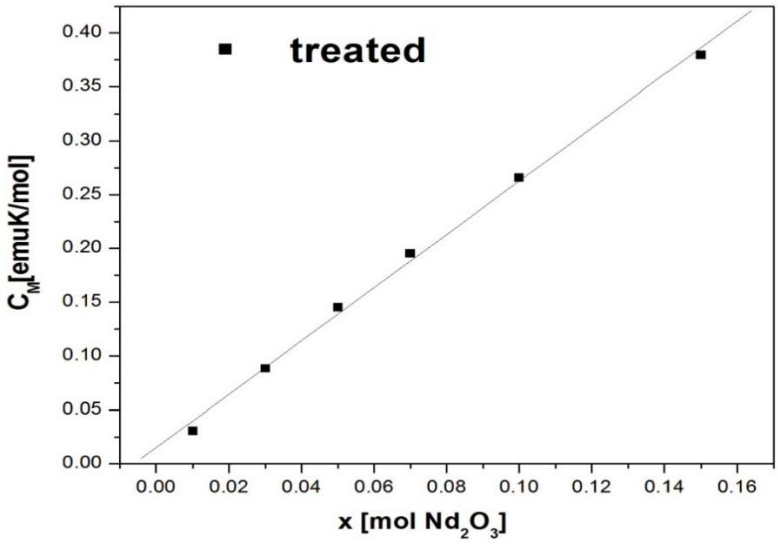

Fig. 6.10. Compositional dependence of the paramagnetic Curie temperature for the heat treated $xNd_2O_3 \cdot (100\text{-}x)[72Bi_2O_3 \cdot 25PbO \cdot 3Ag_2O]$ system.

The behavior of Nd^{3+} ions in the studied samples is tipical mictomagnetic, meaning that Nd^{3+} ions can occur, both as isolated species and as antiferromagnetic coupled with an angle between the magnetic moments. The interaction between ions of neodymium is of super-exchange type, achieved by means of oxygen ions, Nd^{3+}-O-Nd^{3+}.

The compositional evolution of the paramagnetic Curie temperature shows that the number of antiferromagneticaly coupled Nd^{3+} ions increases with increasing concentration of neodymium oxide. For higher Nd_2O_3 content, this process may lead to formation of magnetic clusters.

CHAPTER 7

EXPERIMENTAL RESULTS FOR SYSTEM xRE·(100-x)[4Bi$_2$O$_3$·GeO2] WHERE RE = Gd$_2$O$_3$ AND Eu$_2$O$_3$

7.1. Study of the system xGd$_2$O$_3$(100-x)[4Bi$_2$O$_3$·GeO$_2$]

7.1.1. Electronic paramagnetic rezonance

Adding Gd_2O_3 to the germanium-bismuthate glass matrix enablesEPR spectroscopy investigation of the distribution of gadolinium ions in the vitreous matrix as well as of the microvicinities of these ions. EPR spectra of Gd^{3+} ions in glasses are in grneral anisotropic and are sensitive to changes in the ligand field.

Figure 7.1 shows the RPE spectra of Gd^{3+} ions from the $xGd_2O_3·(100-x)[4Bi_2O_3·GeO_2]$ glass system.

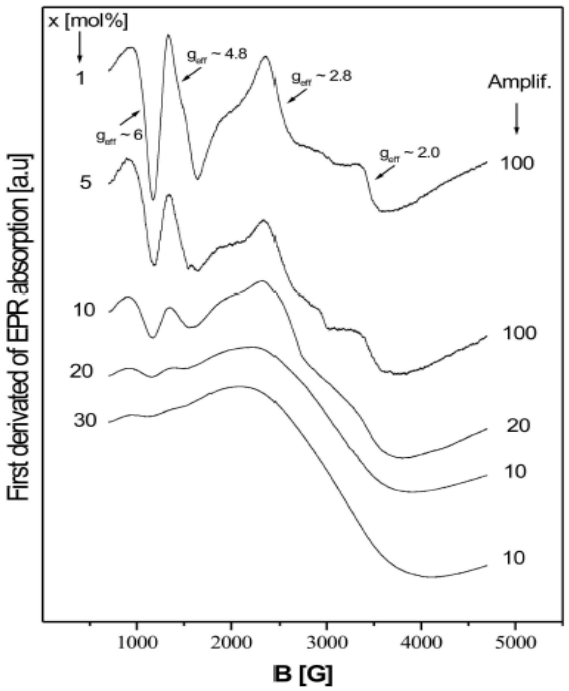

Fig. 7.1. RPE spectra of Gd^{3+} ions from the $xGd_2O_3·(100-x)[4Bi_2O_3·GeO_2]$ glass system.

For low Gd_2O_3 contents ($x \leq 10$), the EPR spectra of the studied samples consists of the resonance signals located at $g_{eff} \approx 6$, 2,8 and 2. This is the so called "U" spectrum characteristic of Gd^{3+} ions localized in positions with weak crystalline fields and of different symmetries (tetrahedral, octahedral, cubic with moderate distortions) having coordination numbers higher then 6. The EPR study of the glasses from the system $xGd_2O_3·(100-x)[4Bi_2O_3·GeO_2]$ shows a distribution of Gd^{3+} ions in two types of locations in the host

vitreous matrix. One of these locations is the one that generates the previously mentioned "U" spectrum. This location is associated with a network modifier role in the vitreous network of gadolinium ions. The second location, characterized by a strong crystal field and low coordination number is associated with a network forming role of gadolinium ions in the vitreous network and is unusual for the gadolinium ions. For a high content of Gd_2O_3 (x>10 mol%), the EPR spectra consist of a single line resonance range, located at geff ≈ 2. This is associated with clustered Gd^{3+} ions.

7.1.2. Magnetic susceptibility measurements

Magnetic susceptibility data complements and support the EPR spectroscopy data.

Figure 7.2 presents the temperature dependence of the reciprocal magnetic susceptibility for the $xGd_2O_3 \cdot (100\text{-}x)[4Bi_2O_3 \cdot GeO_2]$ glass system. For x≤ 10mol% the samples show a Curie type behavior, suggesting that gadolinium ions are mostly isolated and/or participate in dipole-dipole interactions. For x>10mol%, the temperature dependence of the inverse magnetic susceptibility undergoes a Curie-Weiss type behavior with a negative paramagnetic Curie temperature (θp).

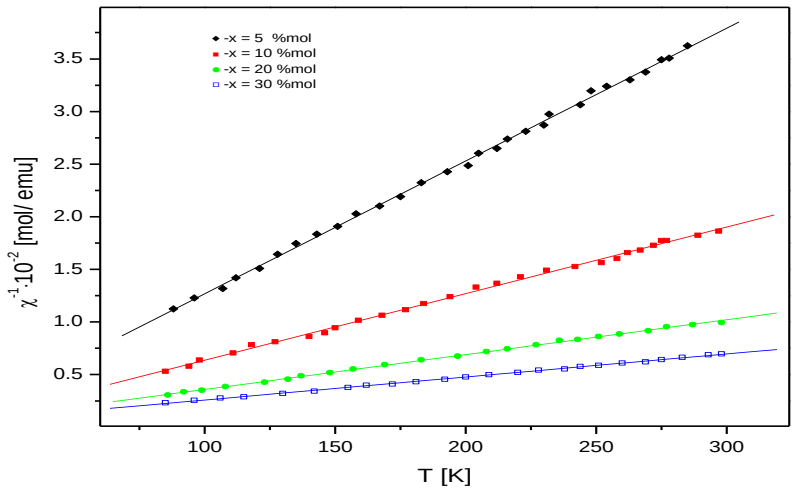

Fig. 7.2. Temperature dependence of the reciprocal magnetic susceptibility for the $xGd_2O_3 \cdot (100\text{-}x)[4Bi_2O_3 \cdot GeO_2]$ glasses.

Fig. 7.3 shows the composition dependence of the paramagnetic Curie temperature (■) and of the molar field constant (o) for the $xGd_2O_3 \cdot (100\text{-}x)[4Bi_2O_3 \cdot GeO_2]$ glasses.

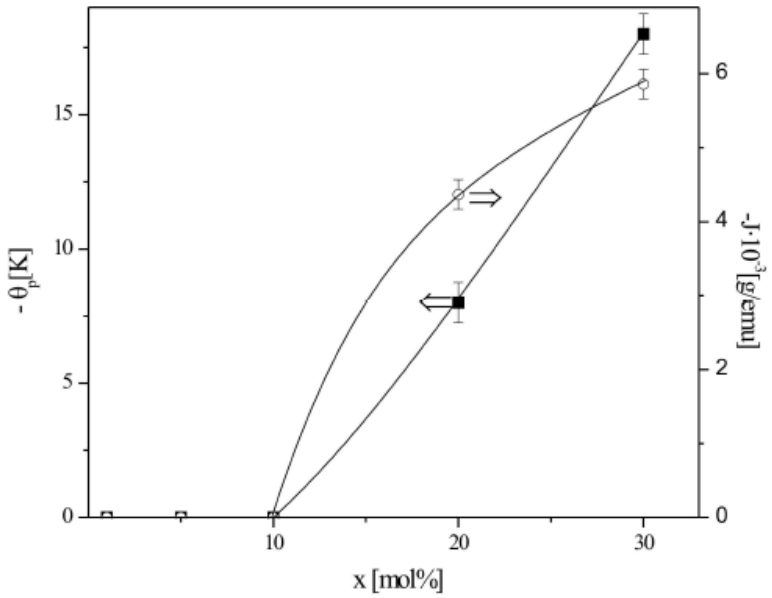

Fig. 7.3. Composition dependence of the paramagnetic Curie temperature (■) and of the molar field constant (o) for the $xGd_2O_3 \cdot (100\text{-}x)[4Bi_2O_3 \cdot GeO_2]$ glasses.

As shown in figure 7.3, for x> 10 mol% the integral absolute values of the magnetic exchange increases when increasing the gadolinium ion content in the studied glass. Magnetic susceptibility data obtained for bismuth-germanium glasses doped with Gd_2O_3 are similar to those previously reported for other oxide glasses containing gadolinium ions and supporting the EPR results presented in this study.

7.2. Study of the $xEu_2O_3 \cdot (100\text{-}x)[4Bi_2O_3 \cdot GeO_2]$ system

7.2.1. X-ray diffraction

Vitreous and/or crystalline nature for the $xEu_2O_3 \cdot (100\text{-}x)[4Bi_2O_3 \cdot GeO_2]$ system with different europium oxides contents ($0 \leq x \leq 30$ %mol) has been tested by X ray diffraction.

After the heat treatment performed at 700°C for 17 hours it was observed the presence of a relatively small amount of crystalline phase. This was analyzed and the presence of crystalline $Bi_4Ge_3O_{14}$ and Bi_2GeO_5 was identified.

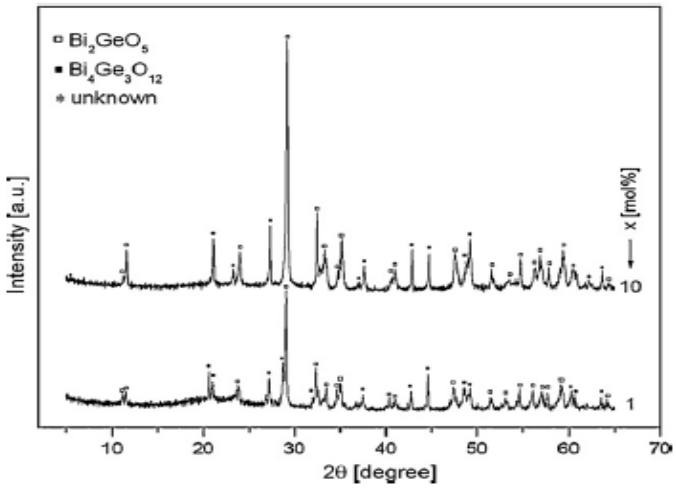

Fig.7.4. Diffractograms for the heat treated $xEu_2O_3 \cdot (100-x)[4Bi_2O_3 \cdot GeO_2]$ system.

7.2.2. IR absorbtion spectroscopy

To determine the influence of the heat treatment on the structure of the studied samples, we compared the FT-IR spectra of as cast samples (Fig. 7.5a) with those of the heat treated samples (Fig. 7.5b). FT-IR spectra for heat treated samples show changes consisting of (1) the narrowing of the absorption band observed for the as cast samples and (2) the appearance of some new bands in the spectra.

Thus, in the FT-IR spectra of the heat treated samples 4 bands appear localized at ~475, ~580, ~680 and ~830 cm^{-1}. The absorption band at ~475 cm^{-1} is assigned to bending vibrations of Bi-O bonds in BiO_3 units. The absorption band at ~830 cm^{-1} is assigned to symmetric stretching vibrations of Bi-O bonds in BiO_3 units. The band at ~580 cm^{-1} is due to the symmetric stretching vibration of Ge-O-Ge bonds. The band at ~680 cm^{-1} is attributed to stretching vibration of Ge-O-Ge bonds in GeO_6 units. The increase of the europium content of the samples produces some changes in the FT-IR spectra. Thus, the band at 830 cm^{-1} disappeares and a new band appears at ~860 cm^{-1}. This suggests a conversion of the BiO_3 into BiO_6 structural units with increasing the europium content of the samples. Thus, the presence of europium ions in the host matrix seems to influence the environment of Bi^{3+} cations favoring the formation BiO_6 units.

The band at 1010 cm^{-1} shifts to the higher wave numbers, namely at ~1020 cm^{-1} and finally become dominant in the IR spectrum.

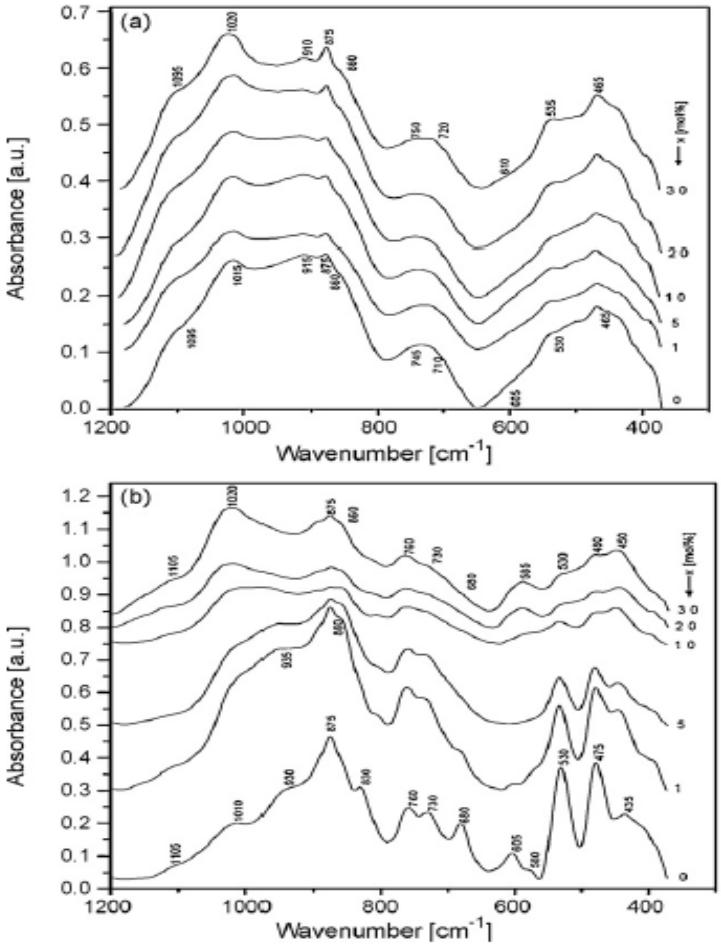

Fig. 7.5. IR spectra for the $xEu_2O_3 \cdot (100 - x)[4Bi_2O_3 \cdot GeO_2]$ samples (a) as cast and (b) heat treated

Structural changes observed by increasing the Eu_2O_3 content of the heat treated samples and evidenced by FT-IR investigations suggests that europium ions play a network modifier role in these samples. The heat treatment induces a process of structural ordering of vitreous network buil up of bismuth (BiO_3 and BiO_6) and germanium (GeO_6 and especially GeO_4) structural units. The IR data suggest that the as cast samples consist mainly of BiO_6 and GeO_4 structural unit while the heat treated samples consist of BiO_3, BiO_6, GeO_4 and GeO_6 structural units.

SELECTED REFERENCES

1. N. F. Borrelli, D. W. Hall, „Nonlinear Optical Properties of Glasses" in Optical Properties of Glass, American Ceramic Society, Westerville, OH, 1991;
2. E. M. Vogel, Phys. Chem. Glasses 32(1991) 231;
3. D. Becherescu, C. Cristea, I. Menessy, F. Winter, „Chimia stării solide", vol.2, Ed. Şt. Enciclopedică, Bucureşti, 1987;
4. I. Ardelean, S. Cora, R Ciceo – Lucăcel, O. Hulpuş, Solid State Sci. 7 (2005) 1438;
5. Y.H.Wang, S.J.Peng, J.D. Lu, R.W. Wang, Y.G. Cheng, Y.L. Maob, Vacuum 83 (2009) 412;
6. R. Ciceo Lucacel, A. O. Hulpus, V. Simion, I. Ardelean, J. Non–Cryst. Solids 355 (2009) 425;
7. T. Matsuura, Y. Abe, Y. Sato, K.Okamoto, M.Ueshige, Y. Akagawa, J. Dent. 25 (1997) 373;
8. L.Baia, M.Baia, W. Kieper, J. Popp, S. Simon, Chemical. Physics 327 (2006) 63;
9. L. Baia, D. Mureşan, M. Baia, J. Popp, S. Simon, Vib. Spectros. 43 (2007) 313;
10. I. Ardelean, V. Timar, J. Optoelect. Adv. Mater. 9 (2007) 840;
11. A. N. Regos, R. Ciceo Lucacel, I. Ardelean, Optoelect. Adv. Mater. 5 (2011) 302;
12. R. Ciceo Lucacel, I. Ardelean, Int. J. Mod. Phys. B 18 (2004) 2915;
13. R. Stefan,S. Popescu, M. Bindea, A. Popa, O. Raita, Scientific Papers: Animal Science and Biotechnologies, 44 (2) 2011,
14. E.Culea, A.Pop, I.Cosma, J. Magn. and Mag. Materials 157/158 (1996) 163;
15. T.Ristoiu, E.Culea, I.Bratu, Materials Letters 41 (1999) 135;
16. E.Culea, I.Milea, J. Non-Cryst. Solids 189 (1995) 246;
17. E.Burzo, I.Ardelean, I.Ursu, Materials Letters 26 (1996) 103;
18. D.Mâţulescu, M.I.Chipară, E.Burzo, I.Ardelean, Phys. Stat. Sol. (a) 161 (1997) 451;
19. S.Sen, R.Rakhmatullin, R.Gubaydullin, A.Silakov, J. Non-Cryst. Solids 333 (2004) 22;
20. E.Culea, I.Bratu, J. Non-Cryst. Solids 262 (2000) 287;
21. S. Rada, E. Culea, **M. Boşca**, M.Culea, R. Muntean, P. Pascuta, *Vib. Spectros.* 48 (2008) 285;
22. P. Pascuta , E. Culea, Mater. Lett. 62 (2008) 4127;
23. T. Ristoiu, E. Culea, I. Bratu, Mater. Lett. 14 (1999) 135;

24. S. Simon, I. Ardelean, Filip S, Bratu I, Cosma I. Solid State Commun. 116 (2000) 83;
25. E. Culea, L. Pop, S. Simon, Mater. Sci. Eng. B 112 (2004) 59;
26. A. Murali, R.P.S. Chakradhar, J.L. Rao, Physica B 364 (2005) 142;
27. K. Nassau, D. Chadwich, J. Am. Ceram. Soc. 65 (1982) 486;
28. C.Lin, J, Opt, Commun, 4 (1983) 2;
29. D. Hall, M.A. Newhouse, N.F. Borelli, W.H. Dumbaugh, D.L.Weideman, Appl. Phys. Lett. 54 (1989) 1293;
30. V. Dimitrov, Y. Dimitriev, A.Montenero, J. Non-Cryst. Solids 180 (1994) 51;
31. P. Beneventi, D. Bersani, P.P. Lottici, L. Kovacs, F. Cordioli, A. Montenero, G.J.Gnappi, J. Non-Cryst. Solids 192–193 (1995) 258;
32. L. Baia, T. Iliescu, S. Simon, W. Kiefer, J. Mol. Structure 599 (2001) 9;
33. Y. Hu, N.H. Liu, U.L.Lin, J. Mater. Sci. 33 (1998) 229;
34. L. Baia, R. Stefan, W. Kiefer, J. Popp, S. Simon J. Non-Cryst. Solids 303 (2002) 379;
35. S. Hazra, A. Ghosh. Phys. Rev. B 51 (1995) 851;
36. P. Pascuta, L. Pop, S. Rada, **M. Bosca**, E. Culea, Vib. Spectros. 48 (2008) 281;
37. E. Culea, J. Non-Cryst. Solids 357 (2011) 50;
38. P. Pascuta, S. Rada, G. Borodi, **M. Bosca**, L. Pop, E. Culea, J. Mol. Struct. 924–926 (2009) 214;
39. S. Rada, P. Pascuta, **M. Bosca**, M. Culea, L. Pop, E. Culea, Vib. Spectros. 48 (2008) 255;
40. L. Pop, E. Culea, **M. Bosca**, M. Neumann, R. Munteam, P. Pascuta, S. Rada, J. Optoelect. Adv. Mater. 10 (2008) 619;
41. S. Rada, P. Pascuta, **M. Bosca**, M. Culea, V. Rus, M. Neumann, E. Culea, J. Optoelect. Adv. Mater. 10 (2008) 3221;
42. C. Kittel, Introducere în Fizica Corpului Solid, Ed. Tehnică, Bucureşti, 1972;
43. I. Ardelean, Introducere în studiul materialelor oxidice cu structură vitroasă, Editura Napocastar, Cluj-Napoca, 2002;
44. M. Avram, Spectroscopia în IR aplicată în chimie organică, Ed. Tehnică, Bucureşti, 1966;
45. E.I. Kamitsos, M.A. Karakassides, G.D. Chyssikos, J. Phys. Chem. 90 (1986) 4528;
46. S. Ram, K. Ram, J. Mat. Sci. 32(5) (1997) 1365;
47. V. Kozhukharov, S. Nikolov, M.Marinov, T.Troev, Mat. Res. Bull. 14 (1979) 735;
48. S. Aştilean, Metode şi tehnici moderne de spectroscopie optică, Vol.I, Ed. Casa Cărţii de Ştiinţă, Cluj-Napoca 2002;

49. N. Avram, Introducere în spectroscopia Raman, Ed. Facla, Timişoara, 1982;
50. A. Butucelea, Tehnici noi în Spectroscopie, Ed. Şt. şi Encl., Bucureşti, 1984;
51. I. Ursu, Rezonanţă Electronică de Spin, Ed. Acad., Bucureşti, 1965;
52. J.L.Rao, A.Muraly, E.D.Rao, J. Non-Cryst. Solids 202 (1996) 215;
53. I.Ardelean, G.Salvan, M.Peteanu, V.Simon, C.Himcinschi, F.Ciorcas, Mod. Phys. Lett. B 13(22-23) (1999) 801;
54. J.Dumas, J.L.Tholence, M.Continentino, J.C.Fernandes, R.B.Guimaraes, J. Magn . Magn. Mat. 226-230 (2001) 468;
55. R.P.S.Chakradhar, A.Murali, J.L.Rao, Optical Mat. 10 (1998) 109;
56. I.Ardelean, H.H.Qiu, H.Sakata, Mat. Lett. 32 (1997) 335;
57. I.Ardelean, Gh.Ilonca, O.Cozar, V.Simon, S.Filip, Mat. Lett. 21 (1994) 321;
58. I.Ardelean, M.Peteanu, V.Simon, S.Filip, F.Ciorcaş, I.Todor, J. Magn. Magn. Mat. 196-197 (1999) 257;
59. M.Peteanu, Teză de Doctorat, Univ. Babeş-Bolyai, Cluj-Napoca, 1989;
60. M. Culea, E. Culea**,** Metode fizice de analiză, Editura Risoprint, Cluj-Napoca, 2004;
61. V. Pop, I. Chicinaş, N. Jumate, Fizica materialelor, Editura Presa Universitară Clujană, 2001;
62. I. Ardelean, Introducere în studiul materialelor oxidice cu structură vitroasă, Editura Napocastar, 2002;
63. Craig A. Merlic, Barry C. Fam and The Regents of University of California Problems in NMR and IR Spectroscopy, http://w3.chem.ucla.edu/%7Ewebspectra/ 1997
64. J. Wong, C.A. Angell, Glass Structure by Spectroscopy, Dekker, New York, 1976;
65. S. Astilean, Metode şi tehnici moderne de spectroscopie optică, Casa Cărţii de Ştiinţă, Cluj – Napoca, 2002
66. I. Ardelean, R. Ciceo–Lucăcel, Fizica şi tehnologia materialelor oxidice, Lucrări practice, Cuj – Napoca, 2000;
67. E. Culea, L. Pop, **M. Bosca**, J. Alloys Compd. 505 (2010) 754;
68. N. Terakado, K. Tanaka, J. Non-Cryst. Solids 354 (2008) 1992;
69. L.M. Sharaf El-Deen, M.S. Al Salhi, M.M. Elkholy, J. Alloys Compd. 465 (2008)333;
70. P. Pascuta, E. Culea, Mater. Lett. 62 (2008) 4127;
71. S. Simon, I. Ardelean, S. Filip, I. Bratu, I. Cosma, Solid State Commun. 116 (2000) 83;
72. P. Pascuta, **M. Bosca**, G. Borodi, E. Culea, J. Alloys Compd. 509 (2011) 4314;
73. E. Burzo, I. Ardelean, D. Matulescu, J. Mater. Sci. Lett. 11 (1992) 1496;
74. P. Pernice, A. Aronne, M. Catauro, A. Marotta, J. Non-Cryst Solids 210 (1997) 23;

75. C. Lin, J. Opt. Commun. 4 (1983) 2;
76. E. Culea, L. Pop, R. Muntean, **M. Bosca**, I. Bratu, M. Bogdan, Mod. Phys. Lett. B 21 (3) (2007) 1;
77. **M. Bosca**, L. Pop, G. Borodi, P. Pascuta, E. Culea, J. Alloys Compd. 479 (2009) 579;
78. L. Pop, E. Culea, **M. Bosca,** R. Muntean, M. Culea, J. Optoelect. Adv. Mater. 9 (2007) 561;
79. P.Y. Shih, Mater. Chem. Phys. 80 (2003) 299;
80. E. Culea, L. Pop, P. Pascuta, **M. Bosca**, J. Mol. Struct. 924–926 (2009) 192;
81. L.G. Sillen, Ark. Kemi Mineral. Geol. 12 (1938) 1;
82. E.Culea, L. Pop, R. Muntean, **M. Bosca**, I. Bratu, M. Bogdan, Mod. Phys. Lett. B 21 (2007) 261;
83. Q. Chen, M. Ferraris, D. Milanese, Y. Menke, E. Monchiero, G. Perrone, J. Non-Cryst. Solids 324 (2003) 12;
84. L. Pop, E. Culea, R. Muntean, M.Culea, **M. Bosca**, J. Optoel. Adv. Mater. 9 (2007) 1687;
85. L.Pop, **M. Bosca**, E. Culea, J. Alloys Compd. 525 (2012) 58
86. P. Pascuta, **M. Bosca**, M. Culea, S. Simon, E. Culea, Mod. Phys. Lett. B 22 (2008) 447;
87. T. Ristoiu, E. Culea, I. Bratu, Mater. Lett. 14 (1999) 135;
88. S. Simon, I. Ardelean, S. Filip, I. Bratu, I. Cosma, Solid State Commun. 116 (2000) 83;
89. S. Simon, R. Pop, V. Simon, M. Coldea, J. Non-Cryst. Solids 331 (2003) 1;
90. E. Culea, L. Pop, S. Simon, Mater. Sci. Eng. B 112 (2004) 59;
91. L. F. Bates, Modern Magnetism, Cambridge University Press, London, 1961;
92. P. Pascuta, L. Pop, S. Rada, **M. Bosca**, E. Culea, Vib. Spectrosc. 48 (2008) 281;
93. L. Baia, T. Iliescu, S. Simon, W. Kiefer, J. Mol. Struct. 599 (2001) 9 ;
94. E. Culea, L. Pop, S. Simon, Mater. Sci. Eng. B 112 (2004) 59;
95. Y. Hu, N.H. Liu, U.L. Lin, J. Mater. Sci. 33 (1998) 229;
96. B. Karthikeyan, Mod. Phys. Lett. B 20 (2006) 533 ;
97. S. Simon, M. Todea, J. Non-Cryst. Solids 352 (2006) 2947 ;
98. M.M. El-Desoky, S.M. Abo-Naf, J. Mater. Sci.: Mater. Electron. 15 (2004) 425.
99. P. Pascuta, **M. Bosca,** S. Rada, L.Pop, E. Culea, J. Optoelect. Adv. Mater. 10 (2008) 2210

SELECTIVE CONCLUSIONS

- The paper presents data on the obtaining, structure and some properties of bismuth-germanium-silver oxide glasses doped with rare earth ions.
- The studied vitreous and vitroceramic systems were chosen due to their interesting physical properties and potential applications. Thus, these systems show a wide range IR transmission, their network is built up by several structural units being possible the interconversion of these units, addition of rare earth oxides produces considerable structural and behavioural modifications, etc.
- The row materials to prepare the studied samples were GeO_2, Bi_2O_3, PbO, Ag_2O, CeO_2, Nd_2O_3, Gd_2O_3 and Er_2O_3 respectively, of analytical purity 99.5%, in the form of powders. The obtained samples were glasses or vitroceramic materials.
- Based on the information obtained by DTA investigation, some of the obtained samples were heat treated at 650°C for 20 hours in order to induce a controlled crystallization process.
- The structure and some properties of the glasses and glass-ceramics from the $xCeO_2 \cdot (100-x)[GeO_2 \cdot PbO]$ and $xGd_2O_3 \cdot (100-x)[GeO_2 \cdot PbO]$ systems with $0 \leq x \leq 15$ %mol prepared by melt quenching were studied. The investigations of the mentioned systems have allowed the obtaining of some important information, as follows:
    - X-ray diffraction data indicate that the addition of CeO_2 to the $GeO_2 \cdot PbO$ host glass matrix triggers the apparition of the $Ce_{1.88}Pb_{2.12}O_{6.53}$ crystalline phase.
    - FT-IR spectra show that the germanium and lead ions act as network forming elemenst, while cerium and gadolinium ions act as network modifiers.
    - The number of GeO_6 structural units increases with the increase of cerium oxide content of the samples.
    - Magnetic susceptibility data show that cerium ions are present in two valence states, 3+ and 4+, the first being the predominant one. With the increase in the cerium content of the samples the Ce^{4+}/ Ce_{total} ratio increases.
- The structure and some properties of the $xEr_2O_3 \cdot$ (100-x) [72Bi2O3·25PbO·3Ag_2O] system were studied.

- The IR spectra of the $xEr_2O_3\cdot$ (100-x) [72Bi2O3·25PbO·3Ag_2O] system show the presence of the BiO and BiO_3 structural units, respectively of the PbO_4 and PbO_3 structural units. The BiO_3 and PbO_4 units amount is bigger for the heat treated samples. For both the heat treated and as cast systems, the number of BiO_6 and PbO_3 decreases in favor of BiO_3 and PbO_4 structural units with increasing the erbium oxide concentration of the samples.
- Erbium ions act as network modifiers in the studied oxide systems.
- In the $xEr_2O_3\cdot(100\text{-}x)[72Bi_2O_3\cdot 25PbO\cdot 3Ag_2O]$ glasses the interaction between the erbium ions is of antiferromagnetic nature consisting in super-exchange interactions realized by means of oxygen ions in coupled pairs of Er^{3+}-O-Er^{3+} type.
- For higher contents of erbium, the interactions between erbium ions lead to the formation of magnetic clusters.

- Glasses from the $xNd_2O_3\cdot(100\text{-}x)[72Bi_2O_3\cdot 25PbO\cdot 3Ag_2O]$ system were obtained and studied. In these glasses, the interaction between neodymium ions is of super-exchange type, achieved by means of oxygen ions through Nd^{3+}-O-Nd^{3+} bonds. With increasing the Nd_2O_3 content of the samples these interactions between neodymium ions lead to the formation of magnetic clusters.
- Glasses of the $xGd_2O_3\cdot(100\text{-}x)[4Bi_2O_3\cdot GeO_2]$ system were prepared and studied. The EPR spectra show the presence of Gd^{3+} ions in two locations of the host matrix, one associated with the network modifier role, the other one associated with a network former role.
- Glasses from the system $xEu_2O_3\cdot(100\text{-}x)$ $[4Bi_2O_3\cdot GeO_2]$ with $0 \leq x \leq 30$ mol% were obtained and studied.
  - X-ray diffraction analysis reveal the presence of two crystalline phases in the vitroceramic samples, namely the crystalline $Bi_4Ge_3O_{12}$ and Bi_2GeO_5.
    - The FT-IR study of the $xEu_2O_3\cdot(100\text{-}x)[4Bi_2O_3\cdot GeO_2]$ system shows that the bismuth and germanium ions play the network forming role while the europium ions play a network modifier role. The vitreous network of the glasses built up of BiO_6 and GeO_4 structural units, while the network of the glass-ceramic samples is constituted from BiO_3, BiO_6, GeO_4 şi GeO_6 structural units.